# THE CORRELATION AND 40AR/39AR AGE DATING OF THE EARLY CRETACEOUS WALKER ISLAND MEMBER BASALTS AXEL HEIBERG ISLAND - CANADIAN ARCTIC

Steven J. Hinds

Submitted in Partial Fufillment of the Requirements
for the Degree of Bachlor of Science, Honours
Dalhousie University, Halifax, Nova Scotia
April 16, 1991

Dalhousie University

Department of Geology
Halifax, Nova Scotia
Canada B3H 3J5
(902) 494-2358

DATE April 16, 1991

AUTHOR Steven J. Hinds

TITLE Correlation and $^{40}Ar/^{39}Ar$ Age Dating of the Early Cretaceous Walker Island Member Basalts Axel Heiberg Island - Canadian Arctic

Degree BSc Convocation May 21 Year 1991

Permission is herewith granted to Dalhousie University to circulate and to have copied for non-commercial purposes, at its discretion, the above title upon the request of individuals or institutions.

# Distribution License

DalSpace requires agreement to this non-exclusive distribution license before your item can appear on DalSpace.

NON-EXCLUSIVE DISTRIBUTION LICENSE

You (the author(s) or copyright owner) grant to Dalhousie University the non-exclusive right to reproduce and distribute your submission worldwide in any medium.

You agree that Dalhousie University may, without changing the content, reformat the submission for the purpose of preservation.

You also agree that Dalhousie University may keep more than one copy of this submission for purposes of security, back-up and preservation.

You agree that the submission is your original work, and that you have the right to grant the rights contained in this license. You also agree that your submission does not, to the best of your knowledge, infringe upon anyone's copyright.

If the submission contains material for which you do not hold copyright, you agree that you have obtained the unrestricted permission of the copyright owner to grant Dalhousie University the rights required by this license, and that such third-party owned material is clearly identified and acknowledged within the text or content of the submission.

If the submission is based upon work that has been sponsored or supported by an agency or organization other than Dalhousie University, you assert that you have fulfilled any right of review or other obligations required by such contract or agreement.

Dalhousie University will clearly identify your name(s) as the author(s) or owner(s) of the submission, and will not make any alteration to the content of the files that you have submitted.

If you have questions regarding this license please contact the repository manager at dalspace@dal.ca.

Grant the distribution license by signing and dating below.

_____ _____

Name of signatory Date

## ABSTRACT

Previous studies have documented the presence of magnetic polarity reversals,which could represent the earliest M0 or M1 reversal of the M-Sequence, in the Early Cretaceous (Aptian-Barremian) sedimentary/volcanic stratigraphic sequence of Axel Heiberg Island. These reversals occur within uncorrelated tholeiitic basalts of the Walker Island Member ot the Isachsen Formation which have within-plate to N-type MORB characteristics. The two main goals of this study are to accurately correlate the basalt units and to then date the determined reversal(s) by the whole-rock $^{40}Ar/^{39}Ar$ procedure. A combination of standard trace element analysis and multivariate statistics (Chernoff's icons) was used successfully to correlate chemically similar flows. Both types of analysis confirm the existence of only one reversal (M0) in the study area. This is the first time icons have been used to represent the chemical relationships in basaltic sequences and the success with this study may encourage future applications.

The results of the whole-rock $^{40}Ar/^{39}Ar$ age analysis provide an age (89-93 Ma), too young for the Walker Island Member that has an Aptian to Barremian (115-125 Ma) paleontological age constraint. One dated sample exhibits an excellent age plateau which is attributed to the argon degassing of a potassium feldspar-bearing crystallization product formed from the original glasses in the sample. As a result, the anomalously young age is interpreted as dating a thermal event which may have coincided with the eruption of the younger (Late Albian to Early Cenomanian) Strand Fiord Formation.

**KEYWORDS**

Chernoff's icons, basalt, Walker Island Member, Isachsen Formation, Strand Fiord Formation, whole-rock $^{40}Ar/^{39}Ar$, magnetic polarity, M-Sequence, M0.

## TABLE OF CONTENTS

# TABLE OF CONTENTS

## CHAPTER 4: CORRELATION OF THE STUDY AREA BASALTS



## CHAPTER 5: RADIOMETRIC AGE OF THE ISACHSEN BASALTS



## CHAPTER 6: CONCLUSIONS



## APPENDICES

## LIST OF FIGURES

## LIST OF TABLES



## ACKNOWLEDGEMENTS

I extend my sincere thanks to Dr G. K. Muecke and Dr D. B. Clarke for their helpful advice during work on this thesis. As well, I would also like to thank Dr. P. H. Reynolds, K. Taylor, and Bob MacKay for their help in this thesis. Funding for this project was provided by the NSERC operating grant and DSS Research Contract by the Institute of Sedimentary and Petroleum Geology (Calgary) to Dr. G. K. Muecke.

# CHAPTER 1: INTRODUCTION

## 1.1 Introduction

In the Early Cretaceous, continental movement of Greenland and Alaska rejuvenated the Sverdrup Basin in the Queen Elizabeth Islands of the Canadian Arctic. Active rifting during this time was the probable cause of the extensive continental basalt eruptions of the Isachsen and Strand Fiord formations (Jackson et al. 1986). The maximum volume estimation of the Sverdrup Basin volcanic rocks is 10,000 to 20,000 $km^3$ (Williamson and Muecke 1989). This thesis deals with the eruption of the basalts of the Walker Island Member of the Isachsen Formation and their significance in refining the age of an important magnetic reversal during the Early Cretaceous.

## 1.2 Location of the Study Area

The study area centres on Bunde Fiord on western Axel Heiberg Island within the Canadian Arctic Archipelago. The three sampled sections examined are: Camp Five Creek (A) Bunde Fiord East (B), and Celluloid Creek (C). These sections lie within a 5 $km^2$ area at the mouth of Camp Five Creek (Fig. 1.1). Rock deformation as a result of the Eurekan Orogeny, and later sediment cover, complicate the field correlation of the basalt flows (Muecke, pers. comm.).

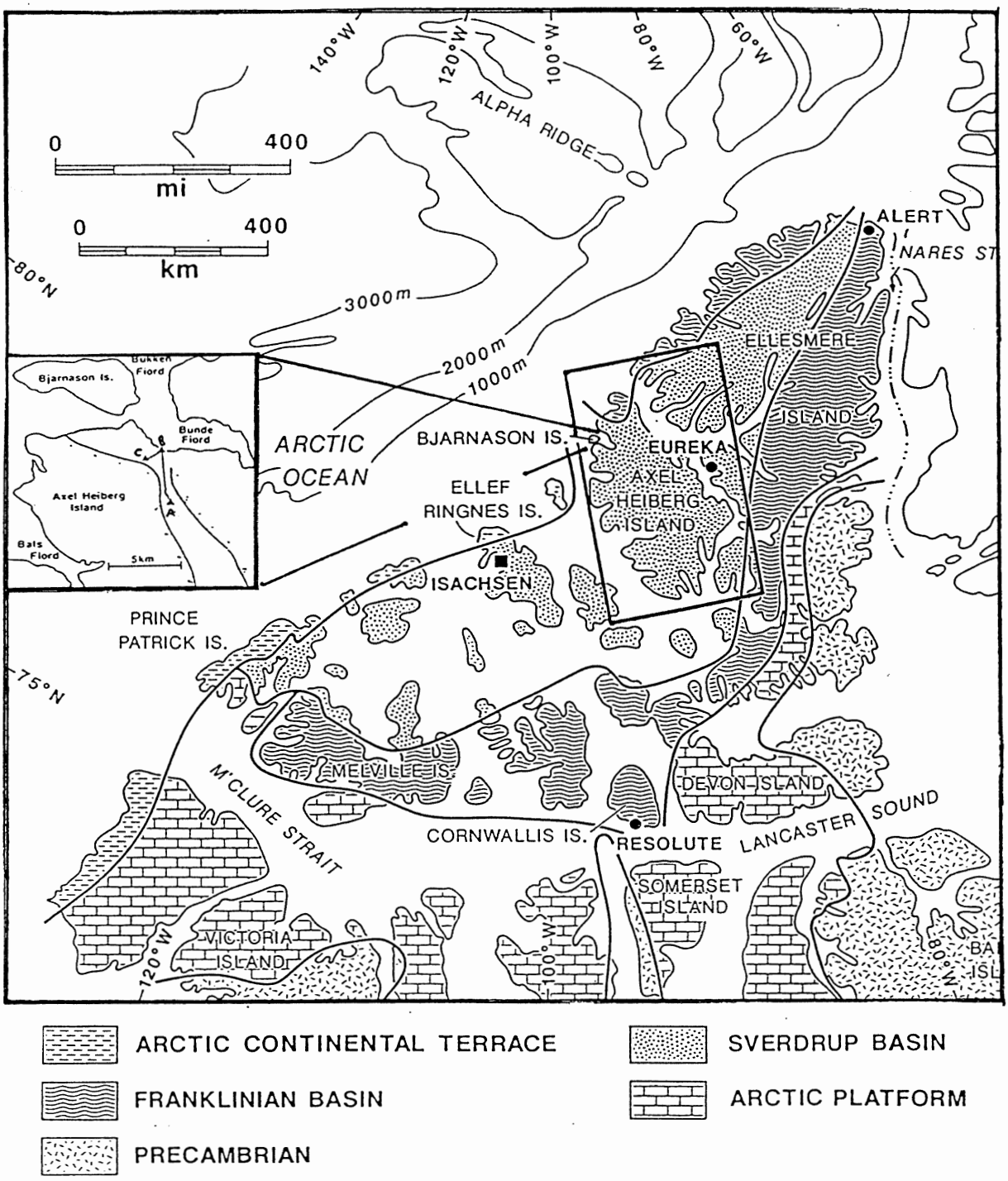


FIGURE 1.1 - Location of the study area in the Sverdrup Basin; Queen Elizabeth Islands - Canadian Arctic Archipelago. (after Embry and Osadetz 1988).

## 1.3 Objectives

This thesis uses field observations, petrographic analysis, and geochemistry, to correlate basalt flows and sequences across the study area. Such correlations test previous conclusions of Wynne et. al. (1988) about the stratigraphic position of reverse polarity basalts (M0) in the study area. Another priority is to date the basalt flows near the reversal by the $^{40}Ar/^{39}Ar$ technique to test the authenticity of previous M0 age estimations.

## 1.4 M-Sequence Reversals and the Magnetic Polarity of the Walker Island Member Basalts

### 1.4.1 The Jurassic - Cretaceous M-Sequence

In the Jurassic to Cretaceous, volcanic and sedimentary rocks record 29 magnetic field reversals of the Earth. The Jurassic-Cretaceous reversals are known as the M-Sequence, and this series numbers from the youngest Early Cretaceous M0 (Aptian-Barremian) to the oldest Late Jurassic M25 (Oxfordian). The first 25 reversals were recorded in rocks produced along the ancient spreading centre between the Pacific and Farallon plates, near the present Hawaiian Islands. The oldest four magnetic reversals (M26-M29) were recorded in rocks encountered in other DSDP drillholes (Ogg et al. 1987) and are beyond the scope of this thesis. Figure 1.2 presents a diagram of the youngest 25 reversals of the M-Sequence. Immediately overlying the M-Sequence is the Cretaceous Quiet Zone which represents a 40 million year

period of normal polarity.

### 1.4.2 The M-Sequence Ages

Paleontologic studies of the sediment overlying the recorded M-Sequence anomalies in the bedrock provide the ages of the Hawaiian reversals (Larson et al. 1975). These studies can only assign a minimum-maximum age interval to the magnetic anomalies. Of the 29 reversals, only M0 (119 Ma) and M25 (156 Ma) have radiometric dates. Kent and Gradstein (1986) estimated the ages of the other magnetic reversals by a plot of the two known radiometric ages and an assumed constant 3.84 cm/yr spreading rate between the Pacific and Farallon plates (Fig 1.2). In Figure 1.2 the absolute ages of the magnetic anomalies can be interpolated from the vertical time scale (Kent and Gradstein 1986). A slight change of the interpolated line slope will affect the ages of the M-Sequence events by about 5 to 10 million years.

### 1.4.3 Age Uncertainties Within the M-Sequence

A fresh, low potassium MORB basalt from DSDP hole 417D (located in the western North Atlantic) defines the $^{40}Ar/^{39}Ar$ date for M0. The DSDP basalts contain less than 0.05 wt% of $K_2O$ and only one sample out of nine (hole 417D core 22) provided reliable results (Ozima et al. 1978). Low potassium contents introduce higher errors because there are lower concentrations of the daughter product $^{40}Ar$ (McDougal and Harrison 1988). The resultant age spectrum for the DSDP

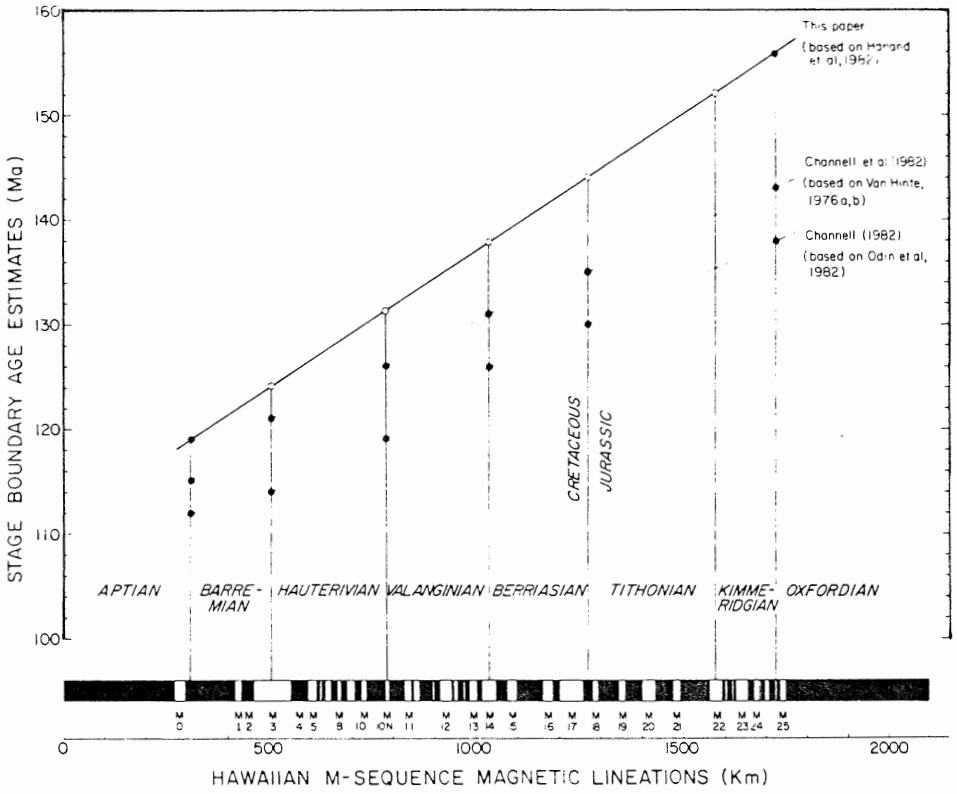


FIGURE 1.2 - The Jurassic-Cretaceous M-Sequence. The two standard points are M0 (119 Ma) and M 25 (156 Ma). The solid line is the present interpretation of the M-Sequence ages with a constant spreading rate of 3.8 cm/yr (after Kent and Gradstein 1986).

basalt is highly irregular with abnormally high ages for the 700 and 1000° heating fractions.

The final 119 Ma age determination excludes the 700° and 1000° temperature fractions and is based on the remaining five fractions (Ozima et al. 1978). The radiometric age for M25 was determined by interpolation of whole-rock K-Ar dates (Armstrong 1978). In general, the age determination for M0 and M25 are unreliable and require refinement using better sample material and improved measurement methods. The continental basalts of the Camp Five Creek location provide an opportunity to improve the dating of M0 since they are relatively fresh and have about 0.6 to 0.9 percent $K_2O$.

The M0 age determination of the Walker Island Member basalts could considerably reduce the uncertainties of the worldwide age assignments to the M-Sequence if they provide an accurate M0 age. A necessary prerequisite of such a refinement is the correct assignment of the magnetic reversal (s) found in the Walker Island Member sequence.

## 1.5 Previous Interpretation of the Study Area

Wynne et al. (1988) measured the stratigraphic magnetic polarity of extrusive volcanic rocks in the Sverdrup Basin and identified two magnetic reversals in the Barremian-Aptian basalt flows of the upper Isachsen (Walker Island Member) Formation (Fig. 1.3). On the basis of poorly constrained stratigraphic evidence, they interpreted these reversals as

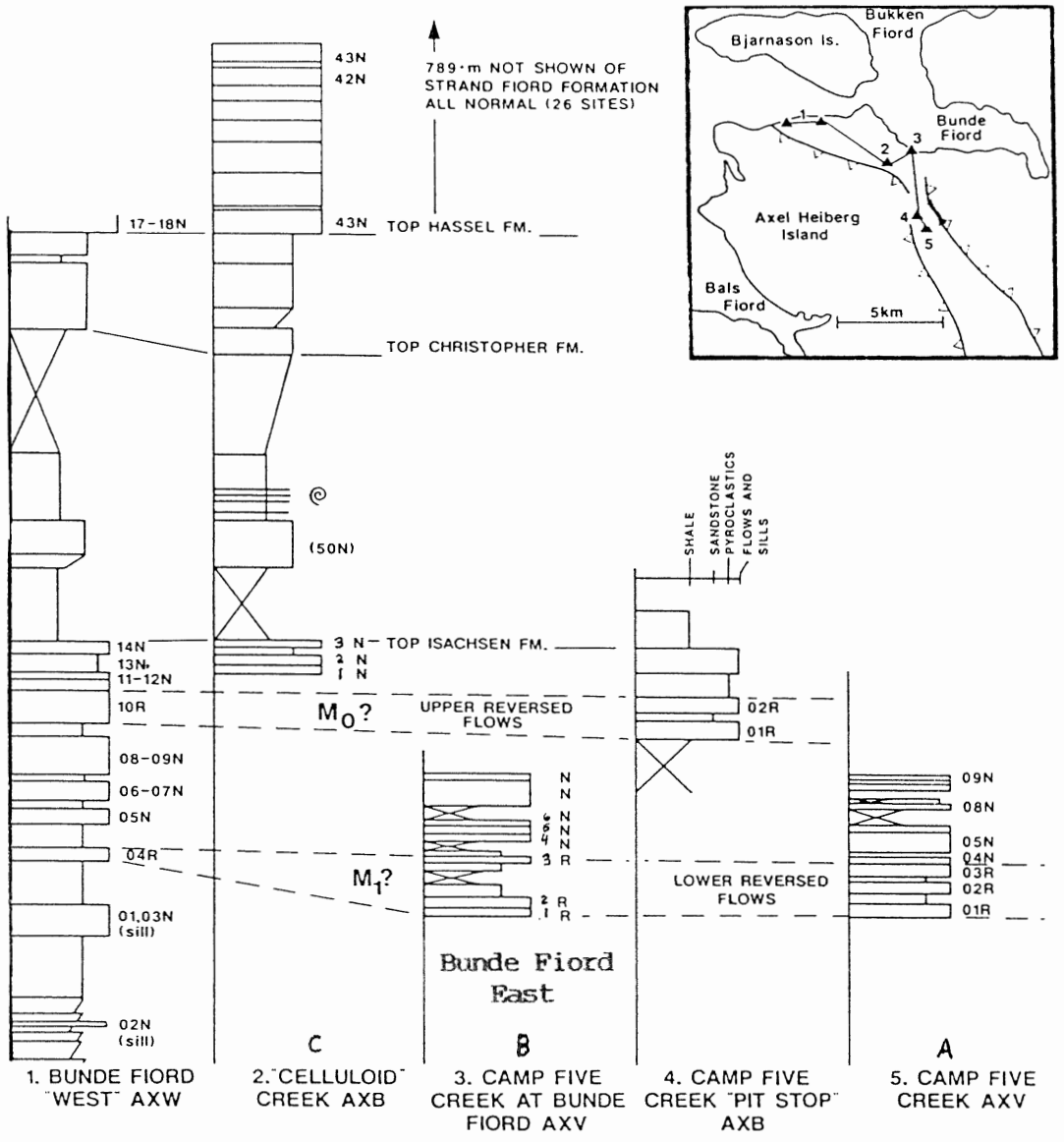


FIGURE 1.3 - Previous stratigraphic interpretation of the Walker Island Member basalts. N - normal flows; R - reverse flows. Note only nine flows in the Camp Five Creek section (A9 - sill) and the absence of flow A10 (after Wynne et al. 1988).

the youngest (M0-M1) reversals of the M-Sequence. The two reversals occur below an extensive 800+ meter thickness of normal polarity basalts of the Strand Fiord Formation. This thick normal polarity formation could represent the Upper Cretaceous Quiet Zone.

Wynne et al. (1988) did not find the reversals in a continuous stratigraphic section, but had to rely on the correlation of a number of discontinuous sections in the study area. They positioned the stratigraphic profiles relative to the reversely magnetized flows (Fig 1.3). New field observations in 1985 and 1990 led to uncertainties in their correlations (Muecke, pers. comm.).

## 1.6 Organization

The first Chapter of this thesis presents the Sverdrup Basin setting and provides a framework for the significance of Walker Island basalts in the evolution of the basin. The second chapter is an outline of the geological setting and tectonic development of the basin. The third chapter uses field, petrographic, and chemical data to classify the basalt sequences of the study area. Next, the fourth chapter is a summary of the basalt unit correlation. The fifth chapter presents the methods and results of the $^{40}Ar/^{39}Ar$ procedure, and discusses the present stratigraphy and implications of the $^{40}Ar/^{39}Ar$ age results. Finally, the sixth chapter is a summary of the thesis conclusions.

# CHAPTER 2 : TECTONIC AND GEOLOGICAL BACKGROUND

## 2.1 Introduction

The Sverdrup Basin has an extensive volcanic and sedimentary history that ranges from the Carboniferous (approx. 370 Ma) to the Tertiary (approx. 45 Ma). Figure 1.1 illustrates the tectonic setting of the Sverdrup Basin. At present, an extensional tectonic model for the Sverdrup Basin is a matter of debate (Williamson 1988, Stephenson et al. 1987).

## 2.2 Tectonic Evolution of the Sverdrup Basin

### 2.2.1 Early Formation and Magmatism

The study area is in the present-day Innuitian Tectonic Province which has four main divisions: the Franklinian Mobile Belt, Pearya Terrane, Sverdrup Basin, and the Arctic Coastal Plain (Trettin 1989). South of the Innuitian Tectonic Province lie the Arctic Platform and Canadian Shield tectonic provinces. The rocks of the Canadian Shield are mainly crystalline basement and sedimentary-volcanic sequences which are Archaen to Cambrian in age (Stephenson 1987). This province is overlain to the north by the Innuitian Tectonic Province and the Cambrian to Cretaceous sediments of the Arctic Platform (Fig. 1.1).

Underneath the Sverdrup Basin are the deformed rocks of the Franklinian Mobile Belt and Pearya Terranes. The cause of

the Franklinian Mobile Belt remains speculative because some of the basement rocks are unknown. However, studies of the extensive Franklin dyke swarm indicate a rifting origin sometime in the Late Proterozoic (0.75 Ga?). The known stratigraphy of the Franklinian Mobile Belt consists mostly of metamorphosed deep water and continental shelf sediments that are Cambrian to Devonian in age (Trettin 1989). During the Ordovician, an exotic continental terrane - Pearya - accreted onto the northeastern corner of the Franklinian Mobile Belt. Pearya has a different crystalline basement than the exposed basement of the Franklinian Mobile Belt. The accretion of Pearya is probably a result of the Mid-Ordovician to Late Devonian Ellesmerian Orogeny (Trettin 1989).

A combination of the Ellesmerian Orogeny and another Early Carboniferous extensional event is the probable cause for the deformation of both terranes. The exact origin of the extension is unknown, but some authors (Trettin 1989) include it within the Mid-Carboniferous to Permian Melvillian Disturbance. Structural evidence from Melville Island indicates that the Sverdrup Basin area was a pull-apart basin between diverging dextral strike-slip fault systems (Trettin 1989).

After the initial rifting and volcanism, the Sverdrup Basin was a deep-water environment and mostly shales dominate in the central areas. At the basin flanks, limestones and shallow-water reefs dominate. Towards the Early Jurassic

extensive sandstones of the Heiberg Formation were deposited. This formation marks the close of the first phase of the Sverdrup Basin development (Stephenson et al. 1987).

### 2.2.2 Tectonomagmatic Rejuvenation in the Cretaceous

Embry and Osadetz (1988) proposed that the second stage of development of the Sverdrup Basin was coupled to the initial rifting and spreading of the adjacent Canada Basin during the Early Cretaceous (Fig. 2.1). The nearby Banks Basin and Englington Graben experienced subsidence at this time. Also, the Sverdrup Rim and Arctic Platform were both uplifted and acted as sediment sources for the subsiding basins. However, the Arctic Platform to the south and east became the main sediment supply for the Sverdrup Basin in the Mid-Cretaceous (Embry and Osadetz 1988).

Extension in the Late Jurassic to Early Cretaceous was probably a result of continental readjustment in the Arctic area. The counterclockwise rotation of Alaska from the Greenland plate initiated rifting in the Arctic Ocean and the formation of the Canada and Sverdrup basins. Extensive submarine(?) volcanic rocks erupted along the now extinct Alpha Ridge near the northern border of the Canada Basin (Jackson et al. 1986).

### 2.2.3 Tectomagmatic Model

The Sverdrup and Canada basins could be parallel rift basins. The initial Sverdrup Basin probably resulted from the

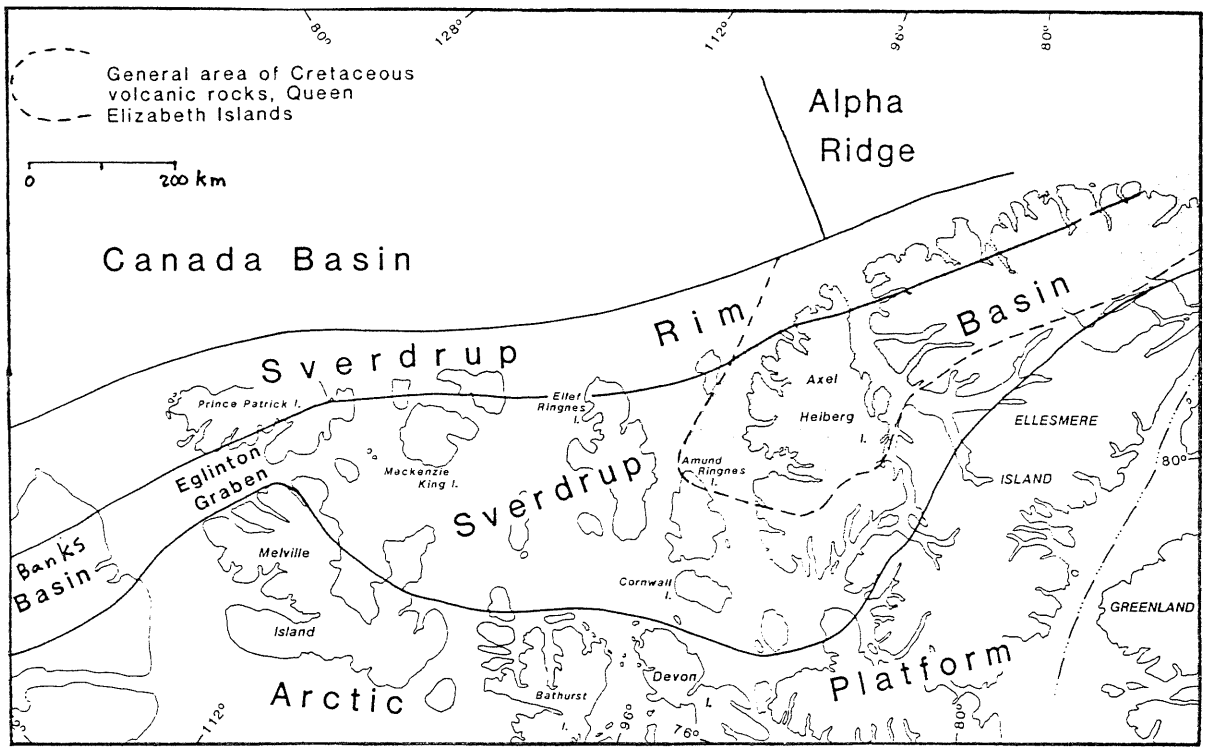


FIGURE 2.1 - Cretaceous tectonic setting of the Sverdrup Basin and distribution of volcanic rocks (after Embry and Osadetz 1988).

Carboniferous Melvillian disturbance which caused upwelling of the asthenosphere (Mutter, et al. 1988). Partial melting of the asthenosphere in the order of 10% occurred beneath the subsiding basin (Fig 2.2a). Support for this asthenospheric upwelling is found in the alkali basalts within the Early Carboniferous Audhild and Borup and the Permian Essayo formations. Trace and rare-earth-element modelling implies a fertile lherzolite (+/-garnet) mantle source for these volcanic rocks (Cameron 1989, Ritcey 1989, Williamson 1988).

After the Melvillian disturbance, thermal subsidence was the dominant crustal activity in the Sverdrup Basin area as the upper asthenosphere cooled. The partially depleted mantle remained underneath the Sverdrup Basin crust as the entire Innuitian Tectonic Province migrated northward during the Late Jurassic (Cameron 1989). Volcanic rocks do not occur in the Late Permian to Late Jurassic strata (Williamson 1988).

The next stage of basin activity began in the Early Cretaceous during the rotation of the Alaskan plate away from the Greenland plate (Fig 2.2b). A second basin formed as the crust failed along a probable weak point caused by the earlier Melvillian disturbance (Mutter et al. 1988). The mantle upwelled once again beneath the mature Sverdrup Basin and the young Canada Basin (Figure 2.2c). The greater degree of asthenospheric partial melting could be the result of a residual from the higher Carboniferous geotherm or small-scale mantle convection (Cameron 1989, Williamson 1988, Mutter et

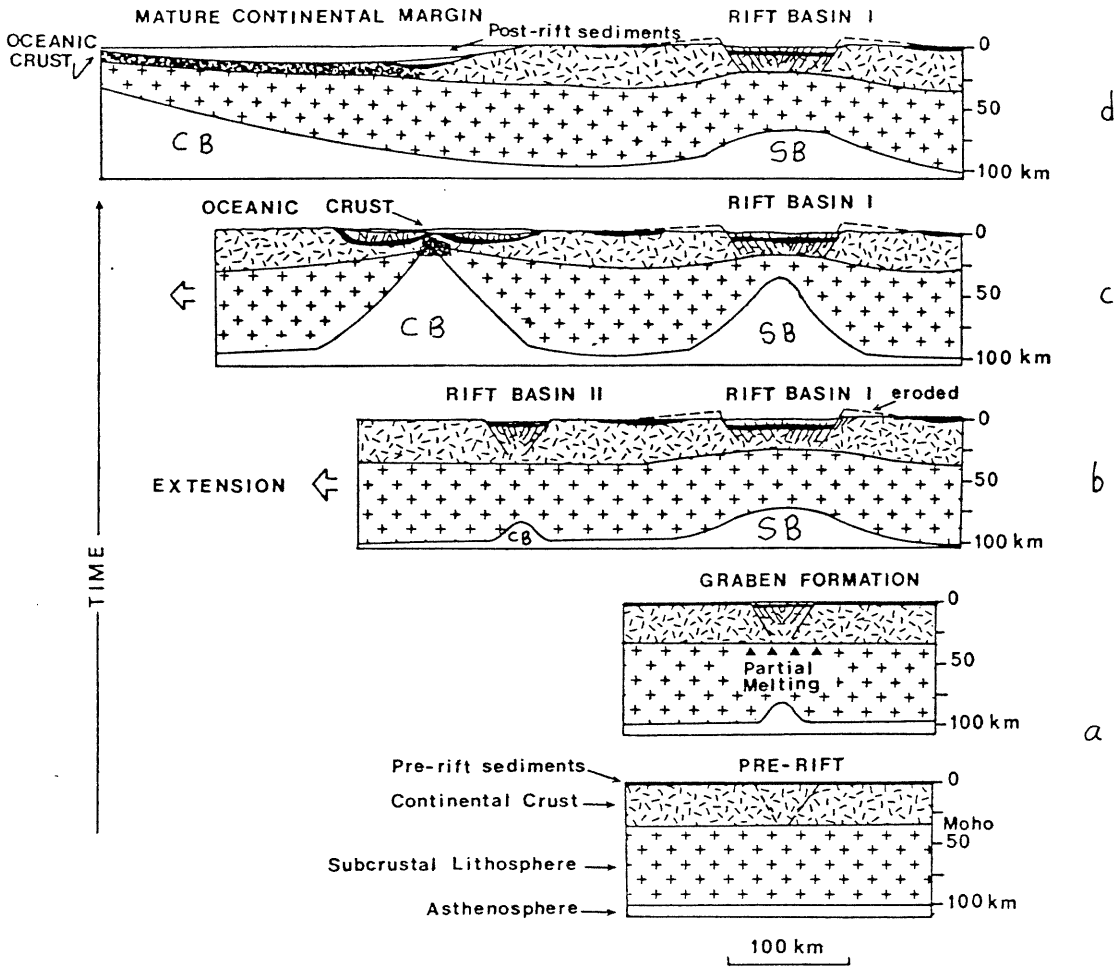


SB = Sverdrup Basin CB = Canada Basin

FIGURE 2.2. Tectonic model for the Sverdrup Basin (after Williamson, 1988)

al. 1988). This episode produced the volcanics of the Isachsen and Strand Fiord formations. At the same time, the crust beneath the Canada Basin failed along a weak point by lithospheric necking (Fig 2.2d), and oceanic crust formed within the Canada Basin during the resurgence of volcanic activity in the Sverdrup Basin (Williamson 1988).

The Cretaceous volcanics of the Sverdrup Basin evolved from uniform composition tholeiites to mildly alkaline basalts. Williamson (1988) proposed a dual fractionation-crustal assimilation model to explain the compositional and isotopic variation in the basalts. Extensive flood basalt eruptions have high turbulent flow rates and the turbulence erodes the cooled magma on the conduit margins in the crust. This results in a greater degree of contact and limited mixing between the ascending magma and the upper crust (Huppert and Sparks 1985).

Near the beginning of the Late Cretaceous, a shift in the zone of extension caused migration of the volcanic centres to the north. The Late Cretaceous basalts are mostly alkaline in nature and probably erupted through thicker crust near the northward rim of the Sverdrup Basin (Muecke 1990). The Cretaceous and older strata of the Sverdrup Basin were subject to compression, uplift, and erosion as a result of the Late Cretaceous to Oligocene Eurekan Orogeny (Trettin 1989).

## 2.3 Stratigraphic Setting of the Cretaceous Volcanics

Four transgressive - regressive cycles of Cretaceous age constitute the Mesozoic succession of the Sverdrup Basin (Embry and Osadetz 1988). The first cycle extends from the Valanginian to Early Barremian and includes the shaly Deer Bay (or Mackenzie King) Formation and the overlying Patterson Island Member of the Isachsen Formation (Fig. 2.3). Three basaltic flows occur among the Patterson Island sandstones on Axel Heiberg Island. These flows are about 10 m thick and are Late Hauterivian to Early Barremian in age (Embry and Osadetz 1988).

The second cycle contains the Walker Island Member basalts which are the subject of this thesis. This cycle extends from the Late Barremian to Aptian and is a combination of the Walker Island Group and Rondon Member of the Isachsen Formation (Fig. 2.3). The Walker Island Member consists mostly of sandstones and tholeiitic basalt flows and is about 300 m thick at Bunde Fiord on Axel Heiberg Island (Fig. 1.3). The greater volume of basalts in this cycle records the main rifting phase of the Sverdrup and Canada basins in this period (Embry and Osadetz 1988, Williamson 1988).

The third transgression-regression cycle of the Sverdrup Basin extends from the Aptian to Early Cenomanian. This cycle consists of the Christopher, Hassel, Bastion Ridge, and Strand Fiord formations. The Strand Fiord Formation has a maximum thickness of 800 m of subaerial and subaqueous basalt

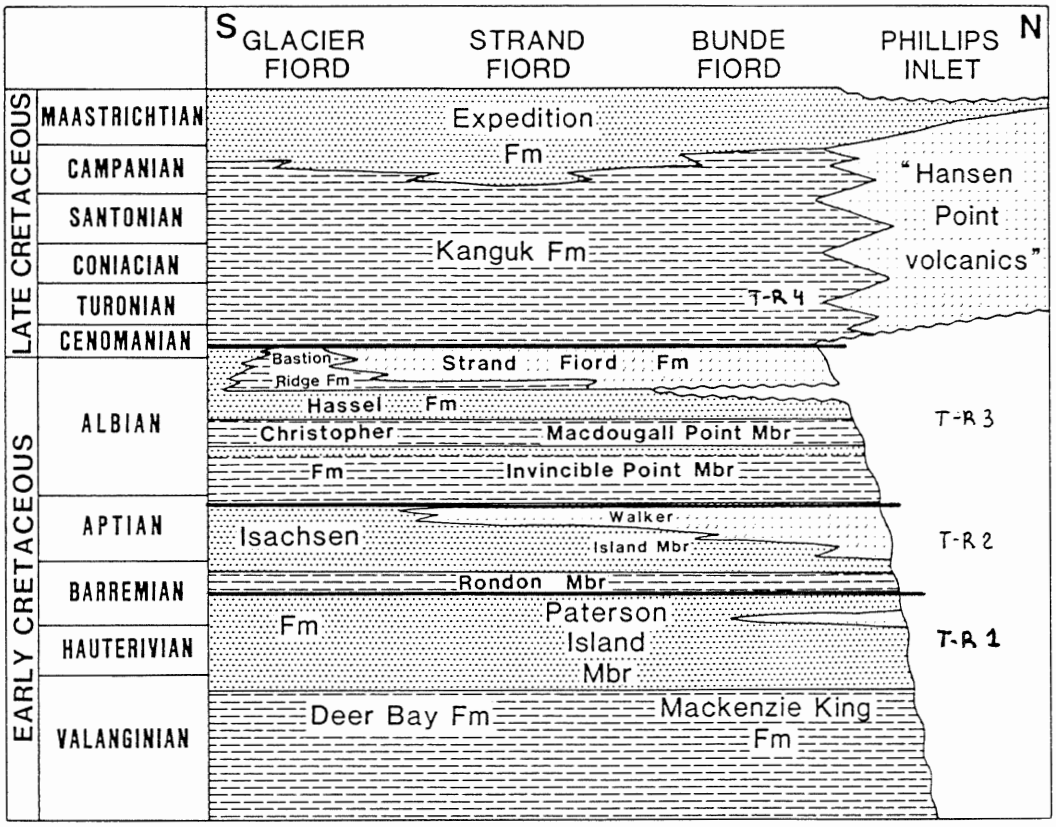


FIGURE 2.3 - The Cretaceous stratigraphy of the Sverdrup Basin; T-R: transgressive - regressive cycles (after Embry and Osadetz 1988).

flows (Embry and Osadetz 1988, Muecke pers. comm.). Also, the Strand Fiord basalts are slightly more alkaline in nature than the Walker Island Member and probably result from fractionation and a small degree of crustal assimilation (Williamson 1988).

The fourth cycle extends from the Late Cenomanian to the Maastrichtian, and is a combination of the Kanguk and Expedition formations. Towards northwestern Ellesmere Island, the Kanguk Formation changes laterally into the Hansen Point Volcanics (Fig 2.3). These volcanics are mostly basalts but rhyolite and trachyte flows are present in some areas (Merrett 1990). The basalt flows are mainly subaerial and the total thickness of the Hansen Point Volcanics is about 350 m at Phillips Point Inlet (Merrett and Muecke 1989).

## 2.4 Stratigraphy of the Study Area

During the 1985 and 1990 field seasons, Dalhousie investigators measured and collected samples from 3 sections of the upper Isachsen Formation in the study area. More favourable weather conditions in 1990 enabled a more complete and comprehensive field examination and re-evaluation of the Camp Five Creek, Bunde Fiord East, and Celluloid Creek volcanics. These are the same sections that Wynne et al. (1988) sampled for palaeomagnetic analysis. The structural effects of the Eurekan Orogeny, plus the variability of volcanic activity, resulted in a lateral stratigraphic discontinuity.

Several faults occur which displace the bottom basalt flow of the Camp Five Creek location. These faults complicate interpretations (Muecke, pers. comm.). Exposure of the steep cliff-face sections is the result of erosion by both Camp Five Creek and Celluloid Creek. Each section has sandstones (Walker Island Member) at the base and recessive interval evidence for shales (Christopher Shales) at the top. The following stratigraphic descriptions are a compilation from field notes by Dr. G. K. Muecke and Mr. R. A. MacRae.

### 2.4.1. Camp Five Creek Section (A)

This is the most complete and accessible section with a total thickness of about 215 m (Fig 2.4). The basal sandstones in this section are generally medium- to coarse-grained and have characteristic low-angle cross bedding intervals with clasts up to 4 mm in size. Quartz-poor horizons among the sandstones contain feldspar grains and coalified plant fragments within a silt to shale matrix. Some sandstones have rare soil and root horizons. The shales of this section usually have thin (20-30 cm) coal horizons and abundant wood fragments up to 20 cm in size. These shales also contain unidentifiable carbonaceous plant fragments.

The basalt flows of this section are usually dense at the base with increasing vesicularity towards the top. One exception is flow A1 which has characteristic vertical vesiculation pipes at the base. These pipes are up to 1 m in height and average 10 cm in diameter. The pipe tops have 20

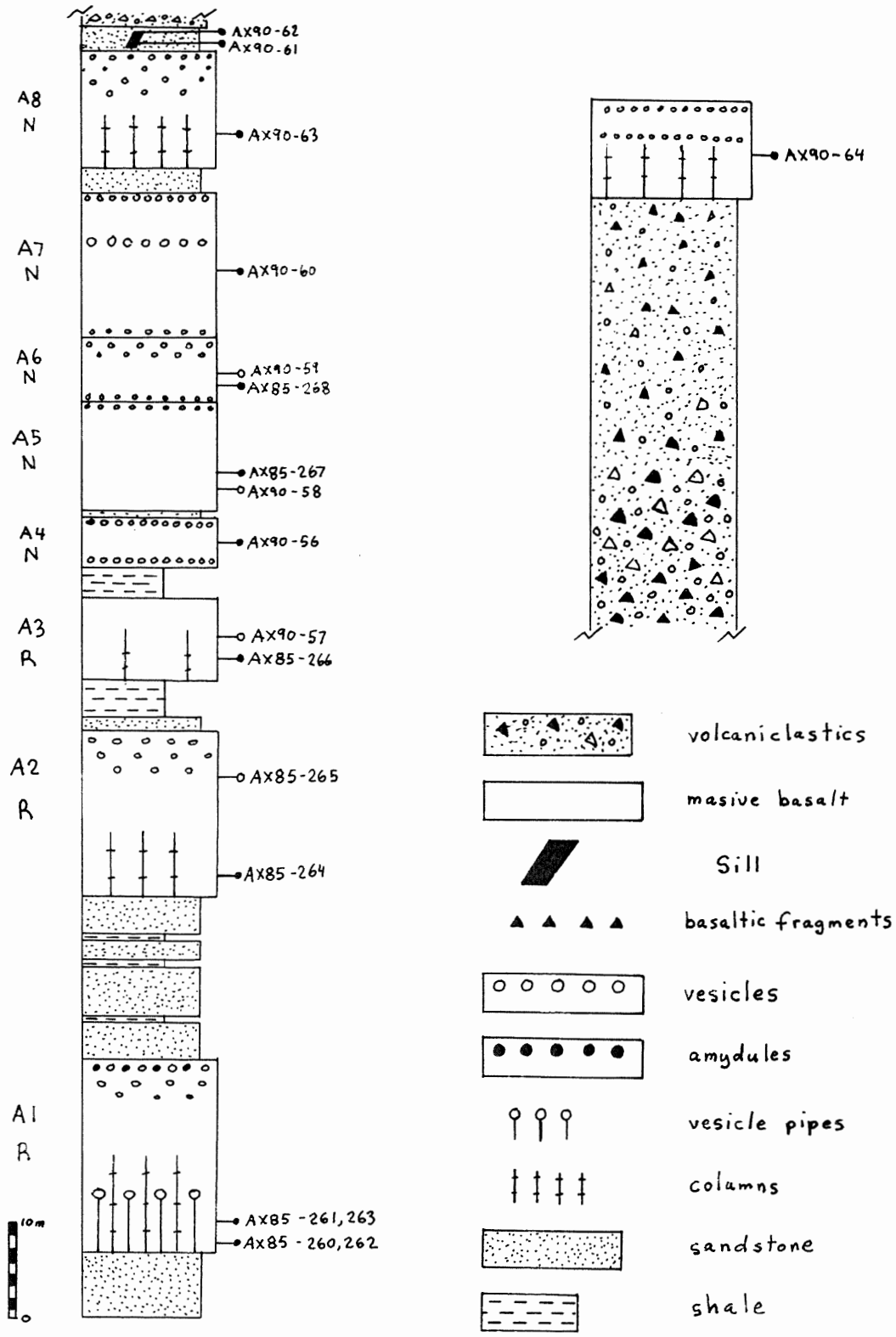


FIGURE 2.4 - Camp Five Creek stratigraphic section.

to 30% vesicles set in a dark green matrix (mafic and oxide minerals?). None of the other flows in this section shows this feature.

Most flows have medium- to well-developed columns at the base and have sharp contacts with the sediments and other flows (Fig. 2.4). Flows A4 and A9 have highly scoriaceous tops as well as top and bottom vesicles. Abundant vesicles in the base of flow A4 suggest that it extruded onto wet sediments and incorporated water vapour. "Flow" A9 is only 1.5 m thick and contains abundant vesicles and calcite vugs along the top half. This unit has chilled margins with the overlying and underlying sediment contacts and is probably a sill. The high abundance of vesicles, calcite alteration, and absence of interstitial glass support this interpretation.

Immediately above the sill are 3 m of light grey sandstones and about 45 m of volcaniclastics. The lowermost 18 m of the volcaniclastics are coarse grained basalt fragments within a sand-silt-mud matrix. Throughout this interval are woody fragments that show some partial sulphide mineralization. From 177 to 204 m, the volcaniclastics have a finer grained texture and are breccias. Large basaltic dykes with chilled margins locally cut the entire volcaniclastic sequence (Fig 2.4).

### 2.4.2 Bunde Fiord East Section (B)

The stratigraphic section in the Bunde Fiord East area

is about 160 m thick but discontinuous. Scree slopes cover important areas between some of the 6 flows (Fig 2.5). The visible sandstones are mostly quartzose and have low-angle cross-bedded horizons. The overall grain size of these sandstones is fine to coarse and bigger 3 mm clasts occur in the cross-bedded horizons. As at Camp Five Creek, the sandstones have abundant coalified plant fragments and possible root horizons. The shales are sometimes carbonaceous and contain coal horizons and plant fragments.

In general, the upper part of the section is poorly exposed and only the massive interiors of the flows are visible. The flows of this section are usually massive at the base with increasing vesicularity towards the top. At 54 m on the section, the base of flow B3 displays poorly developed columns and vesiculation pipes similar to those of Camp Five Creek flow A1. Additional flows could be underneath the scree cover present from 113.5 to 128.5 m in the section. Scoriaceous basalt fragments at 122 m could indicate the presence of a very thin flow. The remainder of the section is below overburden cover.

### 2.4.3 Celluloid Creek Section (C)

The outcrop at Celluloid Creek contains only three basalt flows and one sandstone unit at the base (Fig 2.6). This section is about 22 m thick. The sandstones are medium- to coarse-grained and contain low-angle cross bedded horizons. The basalt flows of this section generally are massive and

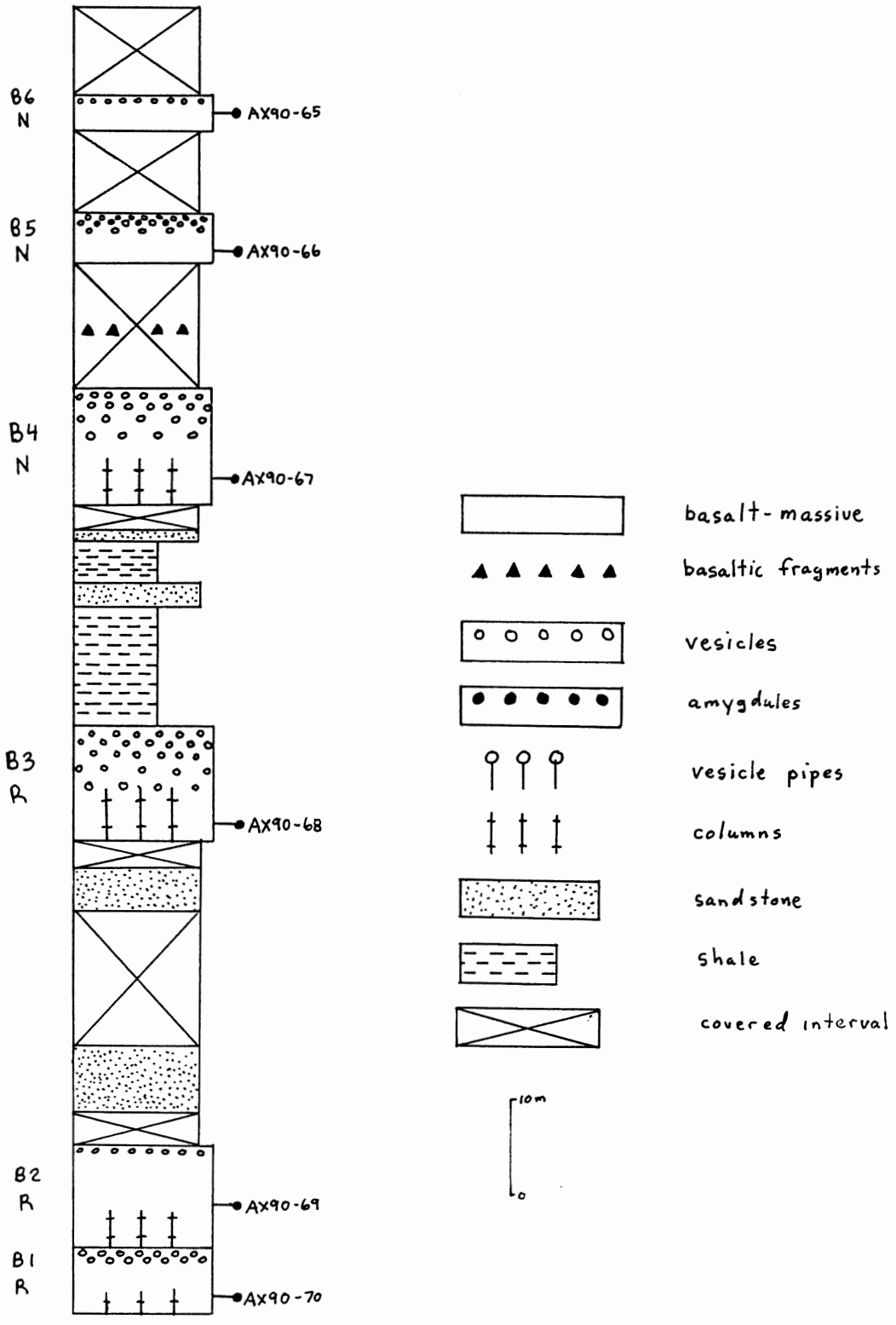


FIGURE 2.5 - Bunde Fiord East stratigraphic section.

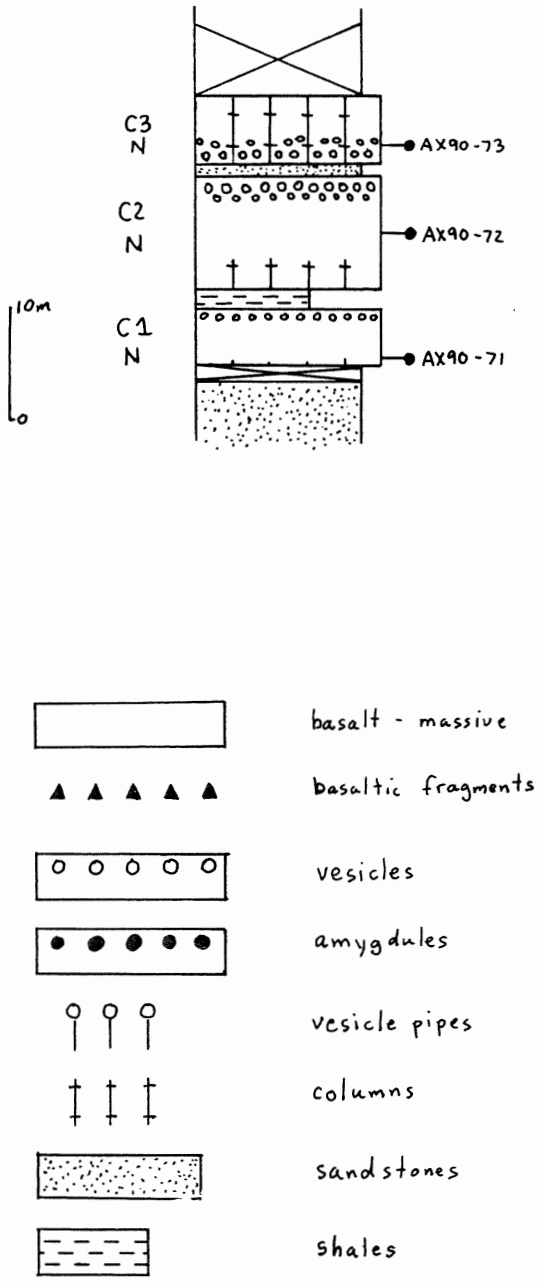


FIGURE 2.6 - Celluloid Creek stratigraphic section

columnar at the bases. Like the other sections, the flows have increasing numbers of vesicles towards the tops. The top of flow C2 is highly vesicular and is overlain by a 50 cm layer of coal with some sulphide mineralization which grades into 30 cm of coal with abundant woody fragments that are up to 20 by 60 cm. The abundance of the woody fragments suggests that flow C3 flowed onto a swampy forest environment in this area.

## 2.5 Summary

In general, the Sverdrup Basin formed from a combination of Early Carboniferous and Late Jurassic-Early Cretaceous extensional events. Extensional events in the Carboniferous and Early Cretaceous produced different compositions of basalt. This could be the combined result of the intensity of each event and the composition of the mantle underneath the Sverdrup Basin. During this time, the continental basalts developed from alkaline to sub-alkaline tholeiites. The study area basalts erupted onto a subaerial delta-plain environment in the Albian-Barremian periods of the Early Cretaceous.

# CHAPTER 3: COMPOSITION OF THE WALKER ISLAND MEMBER BASALTS

## 3.1 Introduction

This chapter uses field observations, petrography, and geochemical analyses (major and trace elements) to classify the basalts of the study area. The geochemical study provides constraints for the interpretation of the origin and development of the Walker Island basalts throughout their eruptive history. An examination of the above characteristics provides the groundwork for the subsequent correlations.

## 3.2 Petrography

The following section summarizes the general petrographic features for the study area basalts. Complete petrographic descriptions of the samples are in Appendix I.

### 3.2.1 Mineralogy and Texture

The basalts characteristically have plagioclase, clinopyroxene (augite), and olivine pseudomorphs as phenocryst phases. By far the most abundant phenocryst phase is plagioclase and its concentration varies from 10-20% by volume. The secondmost abundant phase is augite which ranges from 5-10%. Where present, the modal abundance of pseudomorph olivine is usually 5-7% except 15% in units A10 and C3.

The dominant glomerophyric mineral is plagioclase. Plagioclase forms monomineralic clusters, and also combines with augite and rare olivine. As single grains, plagioclase

is normally in euhedral to subhedral laths and blocky crystals. Clinopyroxene is normally subhedral to anhedral, although euhedral acicular laths characterize some flows. These acicular lath assemblages usually consist of 2-3 crystals. The pseudomorphic olivines are mostly subhedral to anhedral. However, in flows A10 and C3, the individual olivine phenocrysts are essentially euhedral. Most of the plagioclase and some augites display oscillatory zoning.

The groundmass contains plagioclase, clinopyroxene, opaque oxides (titanomagnetite?), interstitial glass, and pseudomorphic olivine. Both high- and low-calcium clinopyroxenes (augite-pigeonite) occur in some basalts. In thin section, the augite has a larger 2V angle compared with the 0-32° 2V of pigeonite (Deer et al. 1985). Pigeonite occurs only in the groundmass, and most samples have groundmass granules that are too small for petrographic analysis. In general, both clinopyroxene and plagioclase are roughly equal in volume percent at 30%.

The groundmass plagioclase occurs mostly as laths and the clinopyroxene and rare olivine are granular. The groundmass glass is mostly intersertal, but is also present in individual pods. Two different types of glass occur in the groundmass: (i) dark brown glass that commonly contains acicular and dendritic oxide intergrowths; (ii) light brown glass that contains blocky oxides. The glass content approaches 20% in some basalts, such as flow C3.

All basalt samples exhibit both glomerophyric and weakly porphyritic textures. Only two units (A5 and B4) have a trachytoid flow texture of the groundmass plagioclases. The glomerophyric clusters range from 1-5 mm in diameter and the individual phenocrysts are about 1-3mm in size. Both are set in a fine- to medium-grained groundmass (0.02-0.5 mm). The groundmass is mostly aphanitic and has a hypocrystalline texture. In some basalts, the cooling was slow enough to permit the formation of a seriate texture between the phenocrysts and groundmass; flow C2 is a good example of this. As well, the phenocrysts exhibit evidence of subsequent growth after eruption in the form of near-rim concentric inclusions.

Only A2, A9, and A10 have significant numbers (10-15%) of amygdules near the flow base which could indicate eruption into wet sediments. However, rare amygdules occur in the middle portions of most flows. Unit A9 has top and bottom chilled margins and about 20% amygdules at the top and bottom sediment contacts. This suggests intrusion into wet sediments and incorporation of volatiles at both the top and bottom. This sill also has a coarser-grained groundmass than adjacent flows which suggests a longer period of crystallization. There is no petrographic evidence of interstitial glass in unit A9.

### 3.2.2 Alteration

Overall, the basalt flows exhibit relatively minor mineral alteration. The only exception is the pseudomorphic

olivines which are altered completely to chlorite and iddingsite. Only flows B1 and C3 have relict olivine near the cores of the pseudomorph grains. Some plagioclase has minor (about 5%) sericite alteration and edge resorption, but most are clear. Clinopyroxenes display little to no alteration.

Most of the secondary replacement occurs in the groundmass glasses and amygdules. In some of the glasses (eg. flow C2) the material has crystallized to a nearly anhydrous intergrowth of quartz and K-feldspar along with the acicular oxides. In most cases however, the major alteration products are clay, carbonate, chlorite, and quartz replacement products. These extremely fine-grained clay minerals are very difficult to identify in thin section. The preservation of most of the primary minerals implies the possible retention of the original geochemical character of the magmas. Flows A5 and A6 (samples AX90-58 and 59) are the freshest with little to no glass alteration.

The thin sill at Camp Five Creek is strikingly different from the surrounding flows and has about 70% alteration of both phenocrysts and groundmass. The main alteration products are carbonate, chlorite, and clay minerals. These alteration products are probably the result of the sill incorporating volatiles from the wet sediments during intrusion.

### 3.2.4 Petrographic Classification

All the basalt samples of the study area have a plagioclase + clinopyroxene + iron-titanium oxides +/- olivine assemblage. This assemblage, plus the low- and high-calcium clinopyroxenes, are characteristic of tholeiite basalts (Hess 1989, Deer et al. 1985).

## 3.3 Flow Correlations using Field and Petrographic Data

The use of mesoscopic field characteristics and petrographic properties for flow-by-flow correlations is beset by many difficulties. For example, the flow texture varies according to the cooling rate and flow thickness. Basalts flowing over wet sediments or swampy areas will cool faster than those erupted on inland sediments. Therefore, the same basalt flow can have different textures and glass concentrations across a near-shore environment (study area paleoenvironment). Paleotopographic highs and lows would control the distribution and thickness of basalts across an area. This could be one of the reasons for the different number of flows in each section across the study area. Thinner basalts are more susceptible to alteration in a flood plain or swampy area.

Furthermore, both field and petrographic studies are biased by the amount of outcrop available (a problem in the study area), and thin section characteristics will be influenced by the location of the sample in the flow (margin

vs centre). Whole-rock geochemical analyses of flows are generally more representative of the entire unit across an area and are more suitable for correlation purposes. The field and petrographic character of the flows are best used to support geochemical correlations.

## 3.4 Whole-Rock Geochemistry

A complete geochemical comparison of the study area basalts is now possible because samples from every unit in the three sections have been geochemically analyzed (Figs. 2.4-2.6). The data set is a combination of previous work (Williamson 1988) and the current study. The new geochemical analyses are presented in Appendix 2. A statistical analysis of repeat samples in the same flow (A1) ensures the reproducibility between the two data sets. Appendix 3 provides a summary of the statistical results. In general, the standard deviations of the repeat samples are below the +/-10% maximum error that may be expected for the XRF analyzer. Therefore, the results from this study can be used in conjunction with the Williamson (1988) data set to determine the magmatic behaviour of the Walker Island Group basalts.

### 3.4.1 Stability of the Major Elements

The concentrations of the major elements (e.g. CaO, MgO, and $Fe_2O_3$) in the Walker Island basalts do not show strong linear relationships in standard Harker plots. In

part, this may be the result of limited mobilization of the major elements when the cooling lava is in contact with aqueous fluids during minor alteration (Wilson 1989). Figure 3.1 includes plots of CaO vs MgO-$SiO_2$ and the data points are in an elongate cluster except for the A9 sill. The independent positions of the sill data could suggest a different fractionation trend from the comagmatic (?) points of the cluster. However, field and petrographic studies clearly show the extremely altered state of the sill and suggest substantial major element mobility in this unit.

Previous studies have shown a transition from subalkaline to mildly alkaline basalt throughout the eruption history of the Sverdrup Basin during the Cretaceous (Cameron 1989, Williamson 1988). The total alkalis vs silica (TAS, Le Bas et al. 1986) plot clearly shows the subalkaline-tholeiitic affinities of the Walker Island Group basalts (Figure 3.2). Because the potassium of the basalts is low (0.15-0.98% $K_2O$) the total alkalies are dominated by $Na_2O$. Hence, mobility of the potassium cannot be detected on this graph.

### 3.4.2 Behaviour of Trace Elements

Incompatible trace element patterns can help determine the source and fractionation of the successive eruptive basalts in the study area. Previous studies show that incompatible elements such as Ti, Zr, Nb, P, and Y have a high ionic field strength and are highly resistant to mobilization by aqueous fluids during alteration (Pearce and Norry 1979).

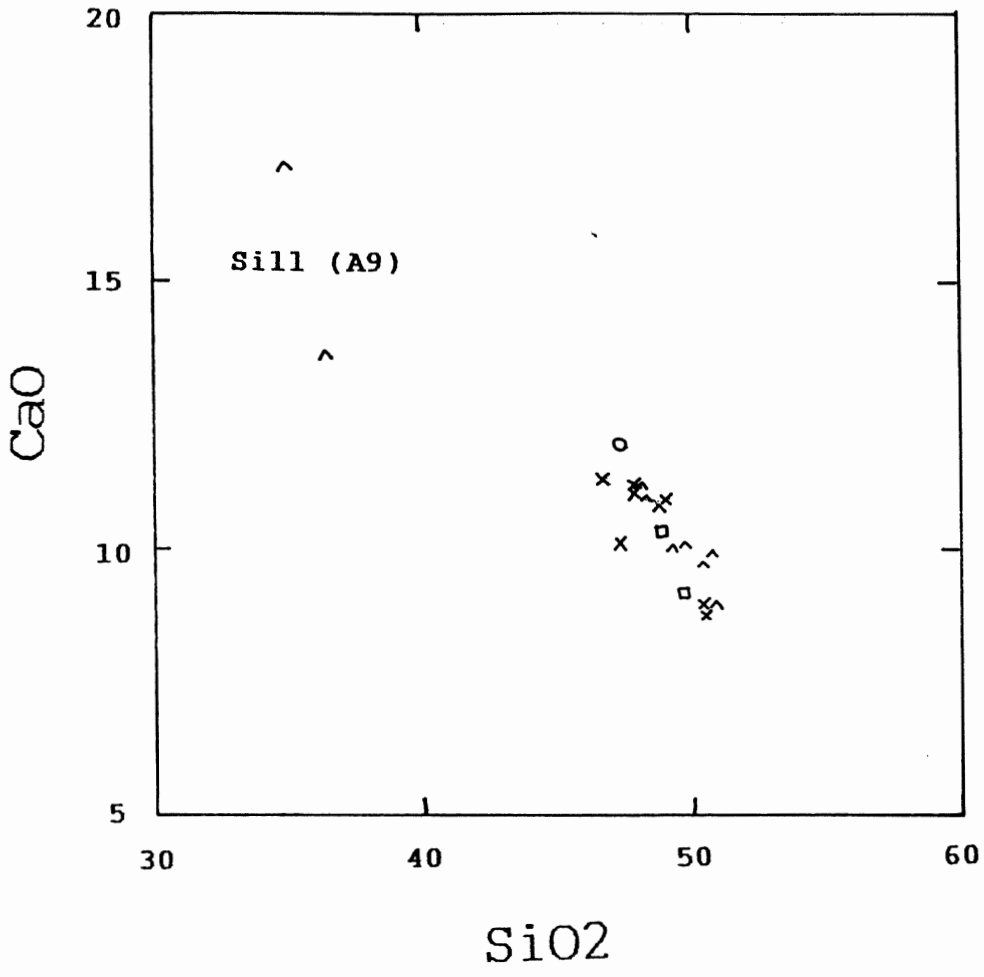


^ - Camp Five Creek
x - Bunde Fiord East
o - Celluloid Creek

FIGURE 3.1a - Plot of CaO against $SiO_2$. The data points show a general CaO increase with decreasing $SiO_2$. All basalts plot within a cluster which is useless for correlation purposes. The altered sill plots outside the main cluster.

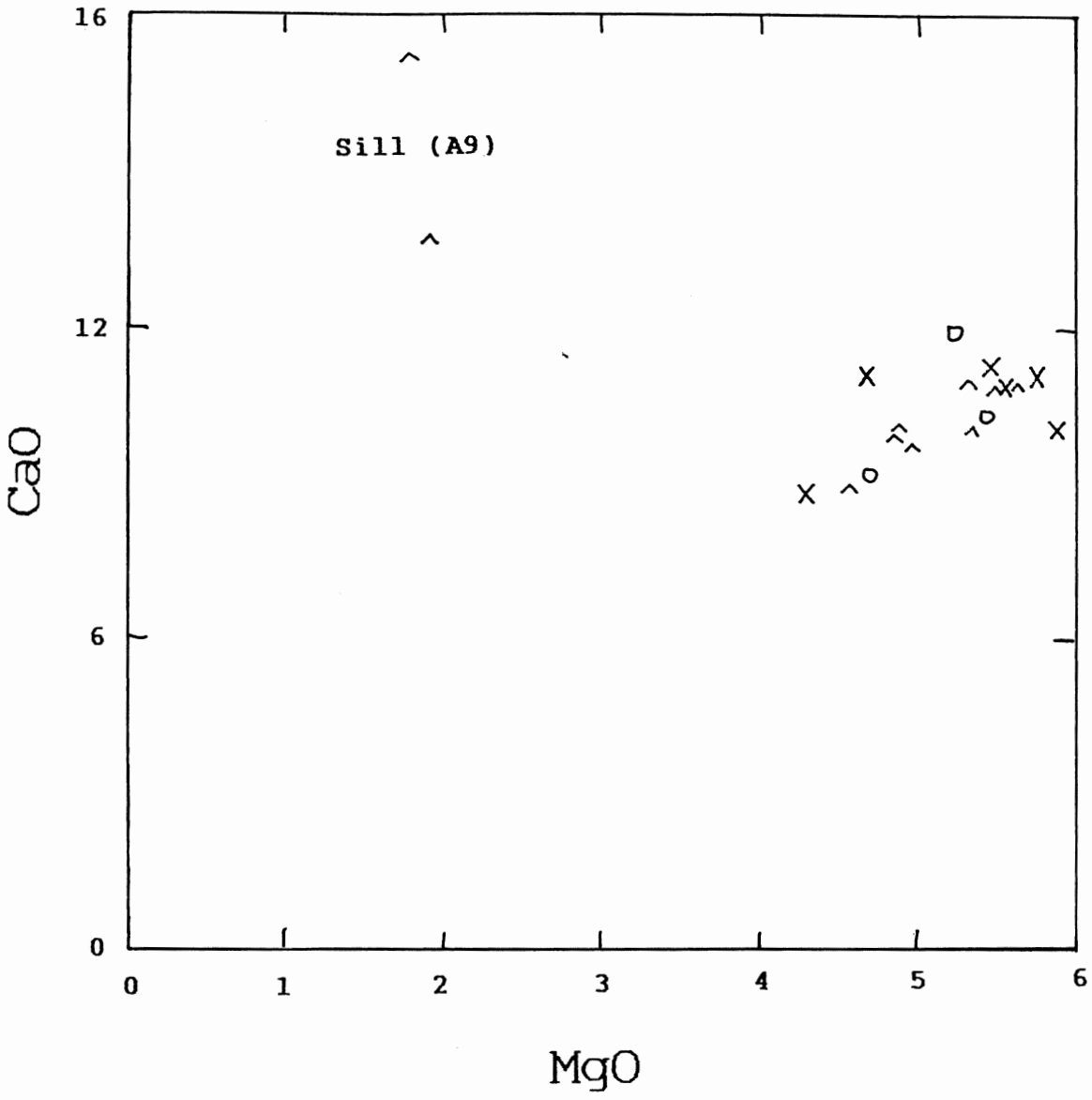


^ - Camp Five Creek
x - Bunde Fiord East
o - Celluloid Creek

FIGURE 3.1b - Plot of MgO against CaO. CaO increases with increasing MgO. Like the plot of 3.1a, the sill plots outside the main data cloud.

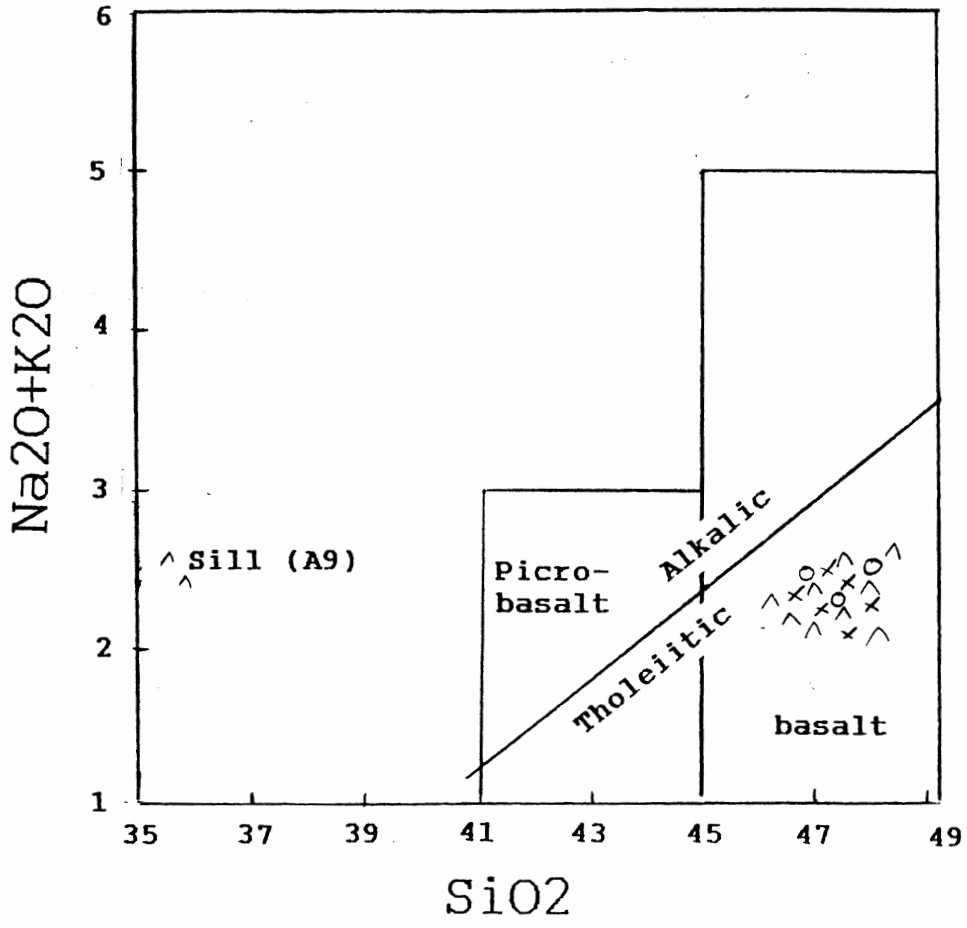


FIGURE 3.2 - The modified TAS classification. All samples except the altered sill plot in a tight cluster within the tholeiitic basalt section (after Le Bas et al. 1986 and MacDonald and Katsura 1964)

In recent studies, both Cameron (1989) and Ritcey (1989) used trace elements to help determine source characteristics in altered basalts.

In a high-level magma chamber of the upper crust, the concentration of incompatible elements in the melt increases as minerals such as plagioclase, clinopyroxene, and olivine crystallize and segregate during fractional crystallization. The concentrations of incompatible elements in successive erupted basalts will, therefore, increase as the volume of melt in the magma chamber decreases and fractional crystallization continues.

Recharge from, and varying degrees of, partial melting in the source region (i.e. upper mantle) causes a periodic increase or decrease in the individual concentrations of the immobile elements in the magma chamber. Recharge introduces additional melt which will generally reduce the concentration of these trace elements in the magma chamber. However, under rare circumstances a low degree of partial melting of pristine upper mantle may produce incompatible element enriched melts that would increase the concentration of the incompatibles in the magma chamber. In the erupted basalts, the concentrations of the incompatibles will vary according to the frequency and intensity of the above processes. However, basalts from the same magma chamber should retain the linear trend and constant (relatively) ratios among trace element throughout the eruption history. Incompatible ratios only vary when magma

mixing or crustal contamination occur which introduces a greater concentration of one incompatible relative to another.

### 3.4.3 Source Characteristics

Using incompatible trace element ratios, Figure 3.3 shows a cluster relationship (sill included) for most of the units. Basalts from all three sample locations fall within the cluster, which implies a similar, comagmatic source. The inclusion of the sill within the comagmatic cluster suggests that the major elements are not reliable indicators of the original composition in this highly altered unit. Two pairs of samples (A5-B4 and A10-C3) fall outside the 92.5% confidence ellipsoid of the Walker Island Group (Fig. 3.3). These pairs are clearly different from the rest and cannot originate from the same magma chamber. The distinction of the pairs could be the result of: (i) magma mixing, (ii) crustal contamination, (iii) different mantle batches due to different degrees of partial melting, and (v) a different parental magma chamber.

If magma mixing or crustal contamination in a single magma chamber is the cause of the chemical difference, then the flows above A5 and B4 should also have similar trace element enrichments and plot outside the trend. Instead, the successive flows above A5 and B4 exhibit very similar ratios to those in the lower parts of the sections. Also, in Figure 3.3 are bulk continental crust concentrations of Nb, Y, and Zr (Taylor and McLennan 1985). The overall values for the bulk

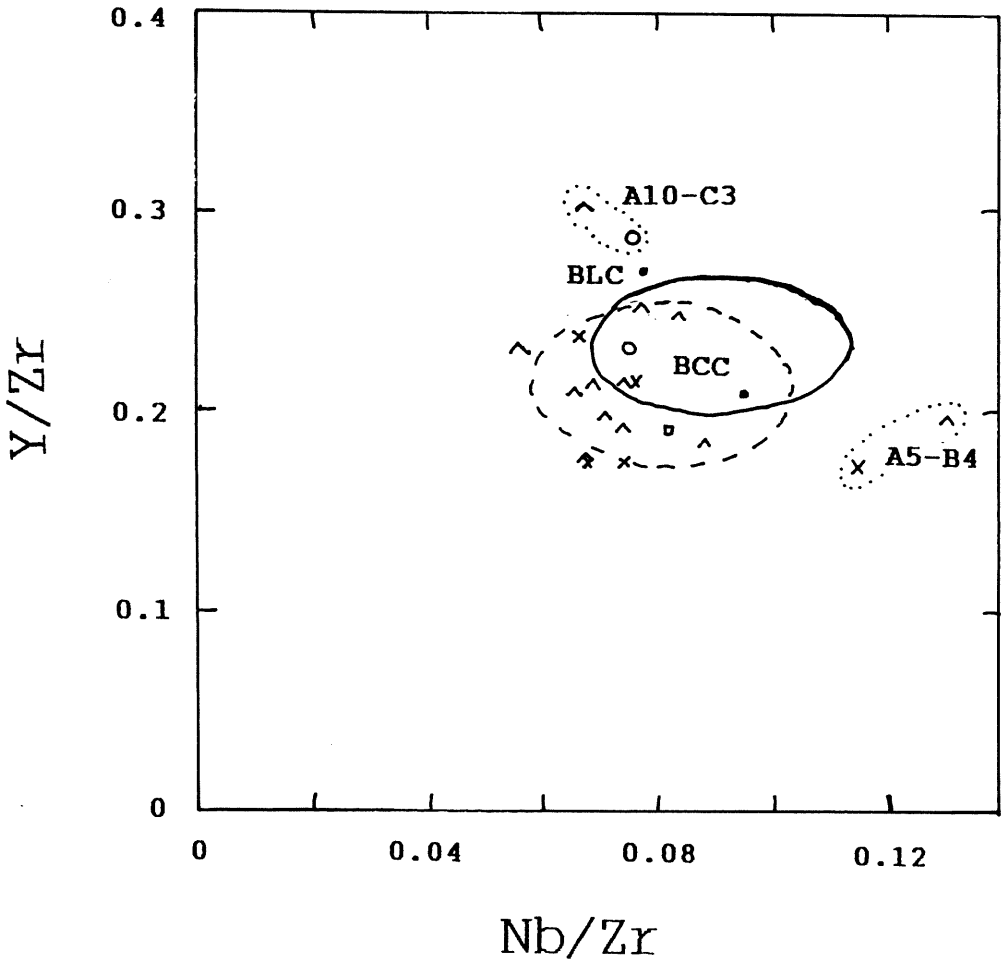


○ - Strand Fiord Fm
◌ - Isachsen Fm
BCC - Bulk continental crust
BLC - Bulk lower continental crust

FIGURE 3.3a - Plot of Y/Zr vs Nb/Zr. Both A5-B4 and A10-C3 plot independent from the main cluster. Bivariate ellipses of both the Isachsen (this study) and Strand Fiord (Williamson 1988) formations are included in an attempt to determine the magmatic affinities of the cluster (see text).

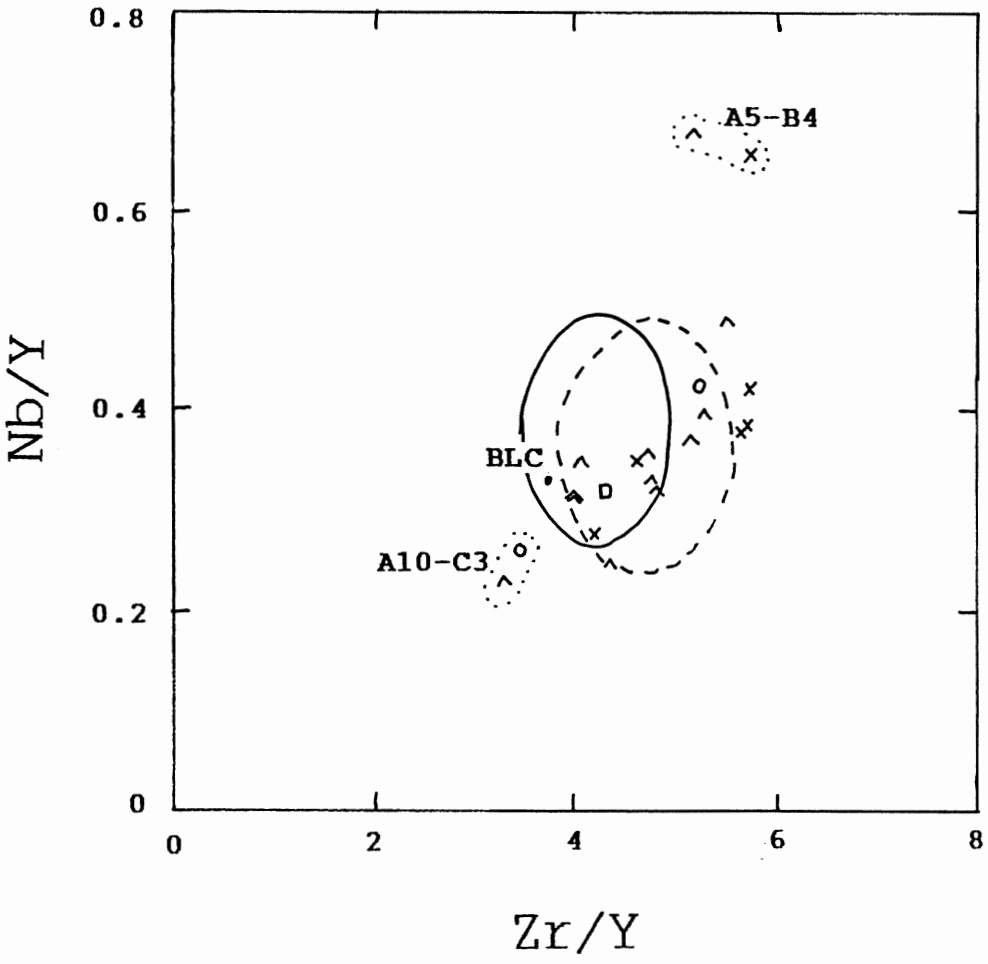


- Strand Fiord Fm
- Isachsen Fm
BCC - Bulk continental crust
BLC - Bulk lower continental crust

FIGURE 3.3b - Plot of Nb/Y vs Zr/Y. Once again A4-B5 and A10-C3 plot outside the data cluster and both ellipses. Bivariate ellipses of both the Isachsen (this study) and Strand Fiord (Williamson 1988) formations are included in an attempt to determine the magmatic affinities of the cluster.

continental crust compositions are lower than the outlying points and cannot explain the enhanced values in A5 and B4.

However, effects of crustal contamination for Walker Island Group basalts are evident in $^{143}Nd/^{144}Nd$ vs $^{87}Sr/^{86}Sr$ isotope plots (Williamson 1988). The evidence above can only exclude extensive assimilation of crustal trace elements by a depleted magma. Crustal assimilation does not explain the relationships in Figure 3.1. Therefore, mixing relationships are not supported by the Figure 3.1 plots. As well, magma mixing between basalts and other more evolved magmas can produce extrusives with different mineralogy and chemical characteristics. However, only basalts with tholeiitic affinities are known to occur in the Walker Island Member (Embry and Osadetz 1988).

The absence of sediments between flows A4, A5, and A6 at Camp Five Creek argues against the possibility of basalt-sediment interaction. Also, these contacts are sharp and do not have reaction surfaces. The chemically different flows (e.g. A5-B4) could be the result of: 1) different rates of partial melting in a homogenous mantle or; 2) similar partial melting in a heterogenous mantle. At present, there is insufficient data available to model the degree of partial melting and the mineralogy of the parental mantle.

The diagram of Figure 3.4a shows a linear relationship controlled by crystal fractionation (plagioclase and clinopyroxene) between all of the units, except for A5 and B4.

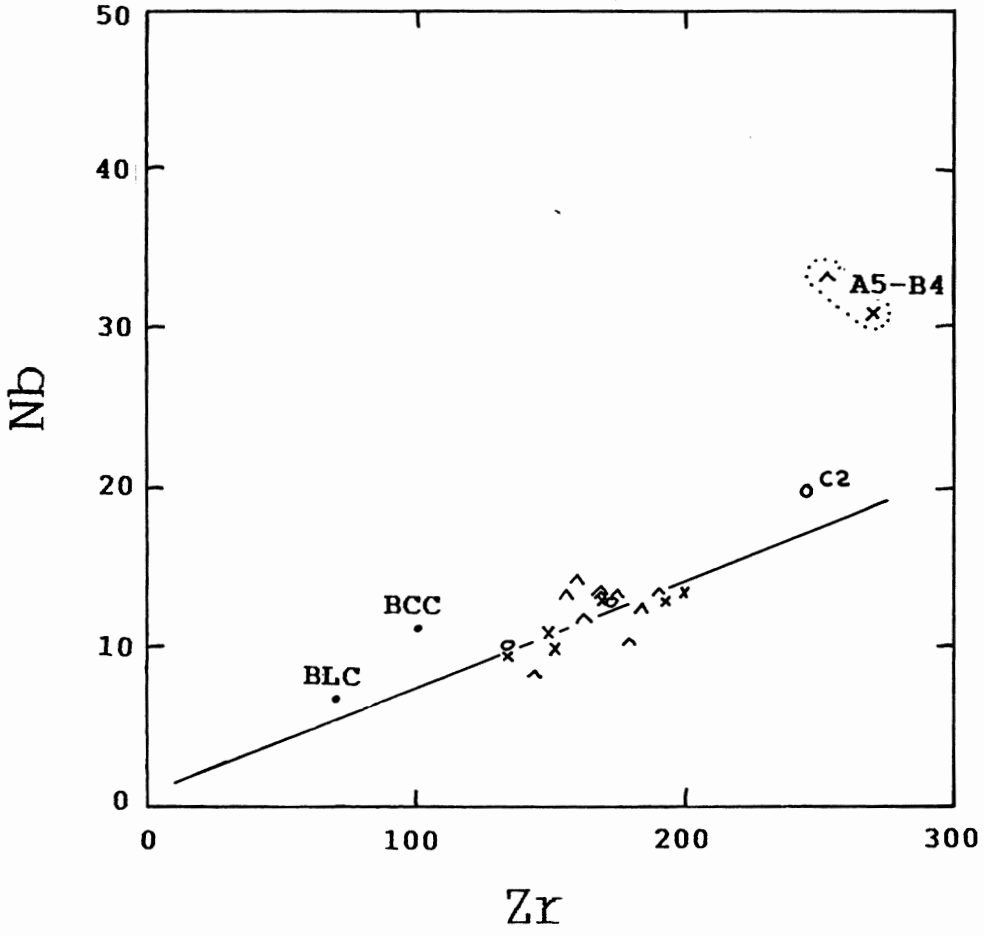


^ - Camp Five Creek
x - Bunde Fiord East
o - Celluloid Creek

FIGURE 3.4a - Plot of Nb vs Zr. Flows A4-B5 and C2 plot outside the linear trend (drawn from origin).

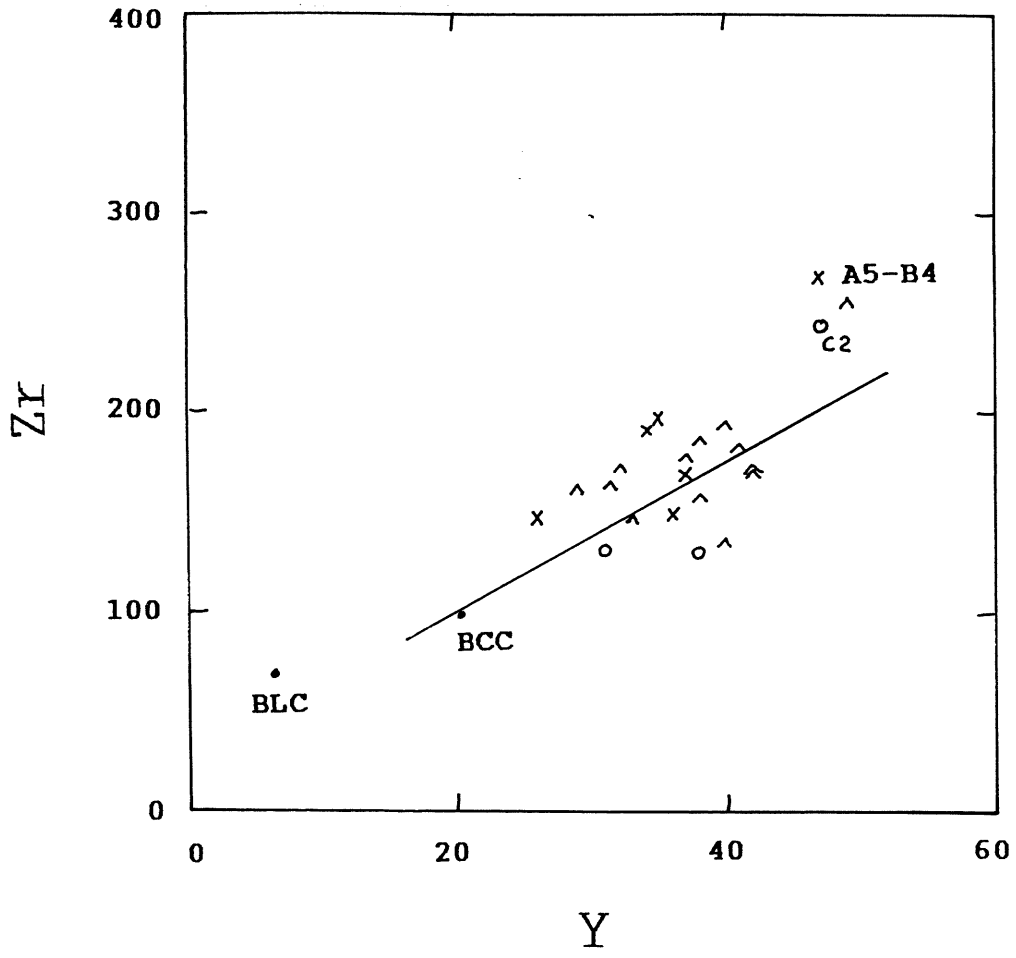


^ - Camp Five Creek
x - Bunde Fiord East
o - Celluloid Creek

FIGURE 3.4b - Plot of Y vs Zr. The minor scatter could be due to limited Y fractionation into clinopyroxene. Flows A5, B4, and C2 plot close together near the top right corner of the graph, independent from the rest of the units.

The greater degree of scatter on the Y-Zr plot of Figure 3.4b could be the result of minor Y fractionation into clinopyroxene. However, this diagram retains the A5-B4 and to a lesser degree, minor A10-C3 distinction from the rest of the flows. The above arguments suggest that the A5-B4 and A10-C3 sample pairs originate from a different magma chamber.

### 3.4.4 Mobility of Potassium

To determine the degree of potassium mobility (from alteration), the potassium concentrations of the basalts are plotted against an immobile element such as Zr (Fig. 3.5). Unaltered basalts should show good linear correlations on potassium vs Zr plots. However, the plot exhibits a considerable scatter which strongly suggests potassium mobility during alteration (Wilson, 1989).

### 3.4.5 Tectonic Discrimination

Pearce and Cann (1973) and Meschede (1986) showed that certain basaltic lavas have trace element ratios that are diagnostic of tectonic regimes. Meschede (1986) uses Nb, Y and Zr - three of the most highly incompatible elements - to distinguish between alkali, transitional, and N-type (depleted trace element) MORBs. Most of the Walker Island basalts plot in the within-plate basalt (WPG) region of the ternary diagram (Fig. 3.6). Once again, flows A5 and B4 are separate from the other samples and plot at the alkali basalt-tholeiite boundary. As well, flows A10 and C3 plot just within the N-

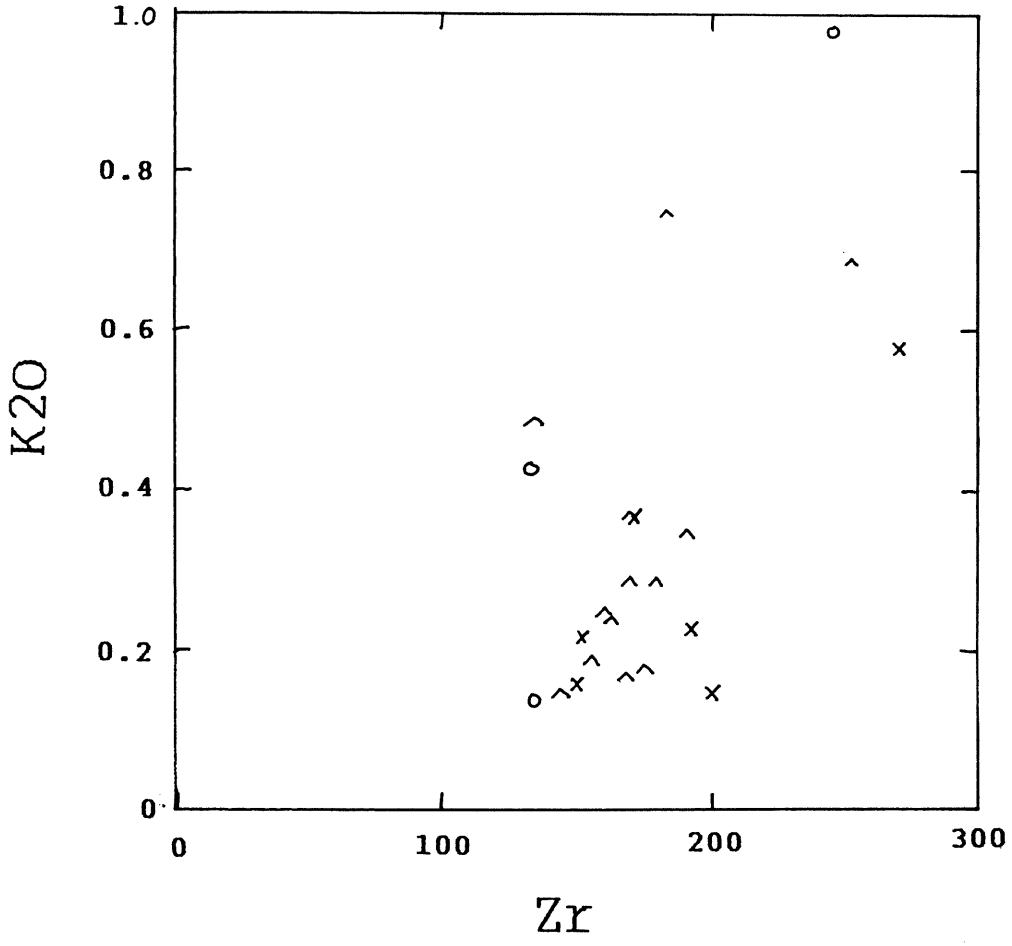


FIGURE 3.5 - Plot of $K_2O$ vs Zr. The data shows a scatter which indicates mobility of the K (Wilson, 1989).

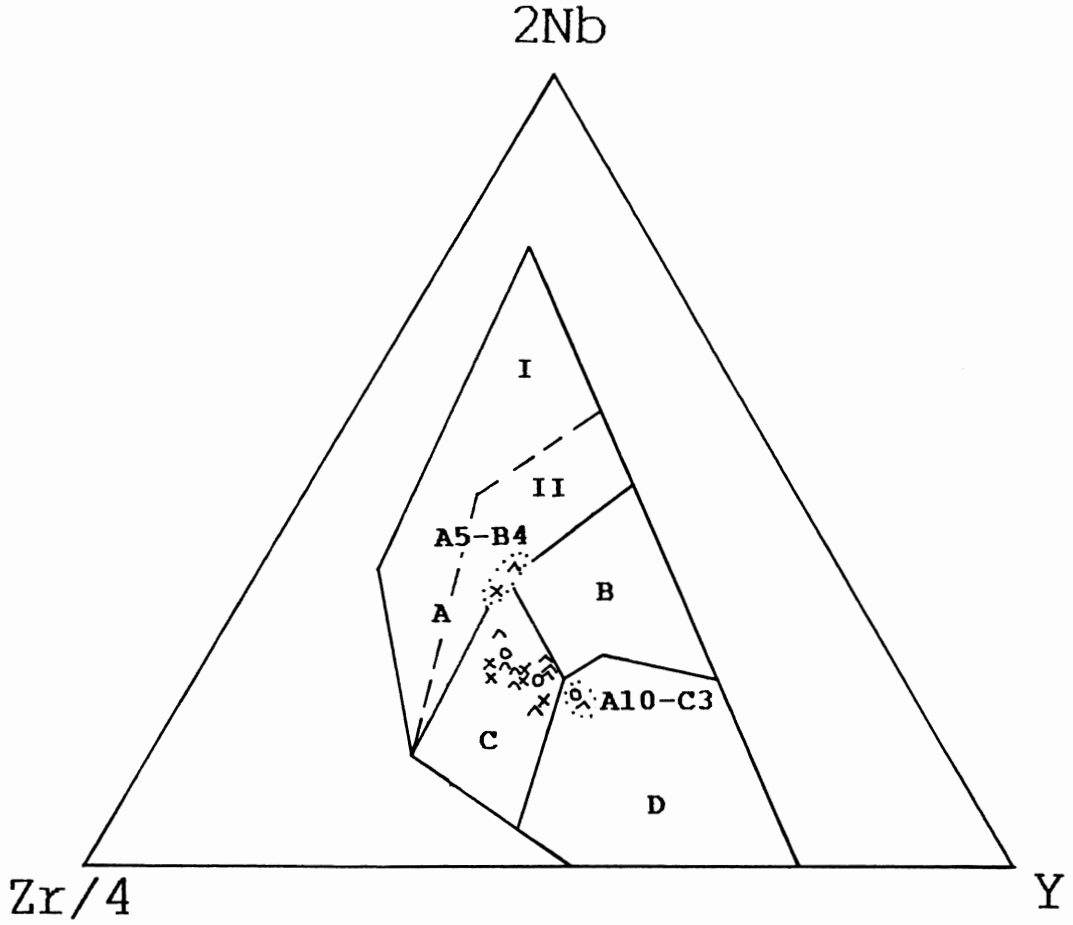


FIGURE 3.6 - Tectonic discrimination plot of Zr-Y-Nb. Flows A4-B5 have a slight alkaline affinity while A10-C3 resembles N-MORBs. AII- within-plate alkali basalt, C- within plate tholeiite, B- MORB, D N-MORB (Meschede 1986).

MORB field and are slightly separate from the others. This indicates the depletion (magmatic source?) of the basalts towards the later eruptive history of the Walker Island basalts. A similar (apparent) depletion trend and the difference in alkalinity of flows A5 and B4 is evident on the $TiO_2$/Y-Nb/Y discrimination plot of Figure 3.7.

### 3.4 Summary

Petrographic and geochemical studies indicate that the Walker Island Member basalts are tholeiitic to slightly alkaline in composition. Most of the basalt flows are comagmatic in origin and flows A10-C3 resemble N-MORBs. Despite extensive alteration, the A9 sill shows incompatible trace element abundances and ratios similar to those of the surrounding flows. Flows A5 and B4 are more alkaline and have distinct incompatible element ratios, probably because they originated from a different magma chamber. Overall, the samples at the three locations (except A5, B4, and C2) appear to be comagmatic and are comparable across the study area.

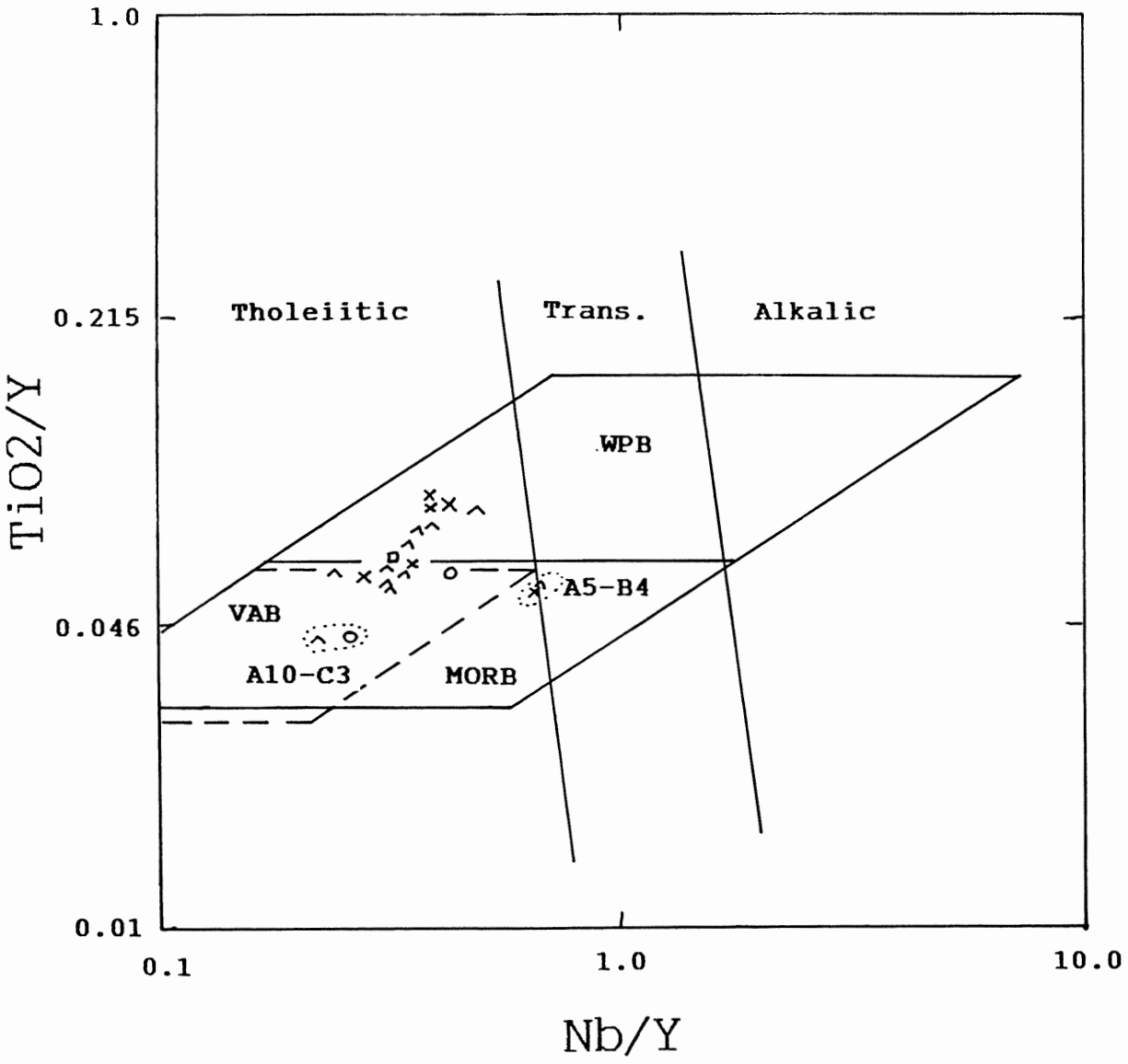


FIGURE 3.7 - Discrimination diagram of TiO2/Y vs Nb/Y. Once again flows A4-B5 and A10-C3 plot independently. VAB - volcanic arc basalt, WPB - within plate basalt (Winchester and Floyd 1975).

# CHAPTER 4 - CORRELATION OF THE WALKER ISLAND BASALTS

## 4.1 Introduction

The lateral distance and absence of outcrop between the sample locations make direct field correlation of the basalt flows impossible. Geochemical correlation of the basalt flows is necessary to determine the stratigraphic position of M0 or M1 in each section. Exposure at Camp Five Creek section is the best and contains the largest number of basalt flows. This section has both normal and reversely magnetized flows and serves as the reference section for the stratigraphic placement of the other sections (Fig. 2.5). Wynne et al. (1988) documented the occurrence of two reversals within the Camp Five and Bunde Fiord East sections. A more precise stratigraphic profile of the study area also places better constraints on the depositional environment and lateral continuity of the volcanics during the Early Cretaceous.

## 4.2 Primary Correlations

The first parameter to consider in the correlation is the vertical stratigraphic sequence in relation to the order of basalt eruption. In most of the cases, the age of the volcanic rocks decreases towards the top of the section. However, complications occur if the basalts erupt or flow into a valley which cuts through older flows. This can result in lateral age differences at the same structural level (Thorpe and Brown 1985).

Magnetic reversals are another useful tool in correlating among the three sections because both Camp Five Creek (A) and the Bunde Fiord East (B) contain reversals. Each location has reversely magnetized flows at the base of the section and this feature prevents the correlation of the upper normal to bottom reverse flows between these areas. In comparing reversely magnetized flows, correlation of different reversals are possible if no other diagnostic features exist.

Another broad correlation exists between the sediment-flow packages of the three sections. In general, both sections A and B have thicker sediment packages and thinner flows at the base. The tops of these sections have a package of thick flows and thinner sediments. The thicker sediment packages have reversely magnetized flows in both locations. The normally magnetized section at Celluloid Creek resembles the thin sediment (thick normally magnetized flows) packages at the top of Camp Five Creek and Bunde Fiord East.

## 4.3 Petrographic and Field Observations

In general, only two tentative correlations (A10-C3 and A1-B3) are supported by both field and petrographic criteria. Flow units A1 and B3 share common vesiculation pipes at the base not observed in any other flow in the three sections. Also present at both flow bases are pipe vesicles (some are bent by flowage). A petrographic feature common to both of these flows is the presence of blocky augite phenocrysts.

Flows A10 and C3 share identical petrographic features such as a glomerophyric-porphyritic phenocrysts set in a fine-grained, granular matrix. The distinctive feature is the presence of euhedral (pseudomorph) olivine phenocrysts which do not occur in any other flow. The final petrographic similarity is the corrosion of the clusters and phenocrysts.

## 4.4 Geochemical Correlation of the Basalt Flows

### 4.4.1 Element Distribution in Basalt Flows

Hetrogeneities may develop in basalt flows as a result of differentiation or local assimilation. These processes primarily affect the concentrations of the major elements such as Fe, Mg, Ca, K, and Na. Flow segregation and crystal settling could concentrate the phenocryst phases in a particular section (middle or base) of the flow. As well, the rate of the above processes could change across the same flow. This complicates the sampling procedure for both petrography and geochemistry. However, in this study immobile trace elements are used which do not readily fit into the crystal lattices of the phenocryst phases.

With the minor exception of Ti and Y, elements such as Nb, Zr, and P do not enter the crystal lattices of the major phenocrysts such as plagioclase, clinopyroxene, and olivine during cooling. The partition coefficient (D = concentration in solid/concentration in liquid) expresses the compatibility of elements in mineral lattices. The incompatible trace

elements above have D < 1 for basaltic minerals (Wilson 1989), therefore, with limited olivine settling, concentrations of these elements remain nearly constant in the melt regardless of segregation or settling. For Y and Ti only a very small percent enters the clinopyroxene lattice. Therefore, moderate amounts of crystal segregation will not affect the overall distribution of these elements in the basalt. Also, the amount of phenocryst clusters is under 20% in all the flows so limited segregation will not substantially affect the trace element concentrations. Field and petrographic observations indicate a relatively uniform concentration of phenocrysts throughout the flows.

Finally, there are no field occurrences of sediment or other xenoliths within the basalts. The sample locations for each of the basalts are in the central portions of the flows, so the effects of any chemical interactions at the margins will not influence the geochemical analyses.

### 4.4.2 Whole-Rock Composition

A sequence of lavas displays nearly identical incompatible chemical compositions and ratios (e.g. Zr/Y) when erupted from a magma chamber that is recharged from the same source. As the volcano (or fissure?) erupts these similar magmas at different times, topography (hills or lava "dams") could prevent the occurrence of flows in some areas. This could lead to apparent stratigraphic correlation of basalt flows that are not time equivalents. Also, multiple volcanoes

fed by the same magma chamber could periodically erupt similar basalts and cause the same incorrect correlations. Trace element ratios (Chapter 3) indicate a single source for most of the flows, and correlation of these basalts is speculative. However, geochemically distinct flow pairs (A10-C3 and A5-B4) act as correlative markers because they show different magmatic affinities.

The most obvious flow correlations are A5-B4 and A10-C3. These pairs plot outside the data cluster of the comagmatic and tectonic discrimination plots of Chapter 3. However, only A5 and B4 are distinctly different on the Figure 3.3 fractionation plots. The most important similarity is the A5-B4 pair which occurs near the middle of the Camp Five Creek and Bunde Fiord East sections respectively (Figs. 2.4-2.5).

In some trace element graphs, C2 plots as an isolated point (Figs. 3.3a and 3.5) but in the plot of Figure 3.3b, this flow is close to A4 and B5. The rest of the flows plot within a cluster and further correlations using bivariate plots are not possible. Overall, the trace element plots of Chapter 3 show two distinct correlations of A5-B4 and A10-B3.

### 4.4.3 Clinopyroxene Composition

To aid the correlation, five samples with augite phenocrysts were analyzed with the electron microprobe at Dalhousie University. Table 4.1 summarizes the mean compositions of clinopyroxene cores for the selected flow

Table 4.1 - Average Clinopyroxene Compositions

| Oxide | (A4) AX90-56 | (A8) AX90-63 | (A10) AX90-64 | (C1) AX90-71 | (C3) AX90-73 |
|---|---|---|---|---|---|
| | N = 14 | N = 14 | N = 17 | N = 15 | N = 10 |
| $SiO_2$ | 52.75 | 51.73 | 51.42 | 51.28 | 52.60 |
| $TiO_2$ | 0.57 | 0.75 | 0.68 | 0.80 | 0.57 |
| $Al_2O_3$ | 2.06 | 2.88 | 3.05 | 2.95 | 2.45 |
| $Cr_2O_3$ | 0.19 | 0.10 | 0.21 | 0.04 | 0.25 |
| FeO | 8.47 | 8.79 | 10.00 | 9.34 | 9.82 |
| MnO | 0.22 | 0.21 | 0.25 | 0.23 | 0.24 |
| MgO | 16.51 | 15.54 | 15.89 | 15.35 | 16.46 |
| CaO | 19.53 | 19.93 | 18.30 | 19.60 | 17.68 |
| $Na_2O$ | 0.24 | 0.27 | 0.23 | 0.28 | 0.20 |
| | | | | | |
| Total | 100.38 | 100.20 | 100.00 | 99.87 | 100.29 |

samples. Not all flows were examined because of time constraints and the absence of sufficient augite phenocrysts in some polished thin sections. Therefore, these results can only supplement the previous determinations. An average of four clinopyroxene cores with four analyses (N) were determined per sample; Figure 4.1 presents the average composition plots for flows A5-B4 and A10-C3. There is an overlap between the clinopyroxene compositions for all flows and definite correlations using clinopyroxene compositions cannot be made at this time.

**4.5 Multivariate Statistical Analysis**

In an ideal situation, geochemical flow-by-flow

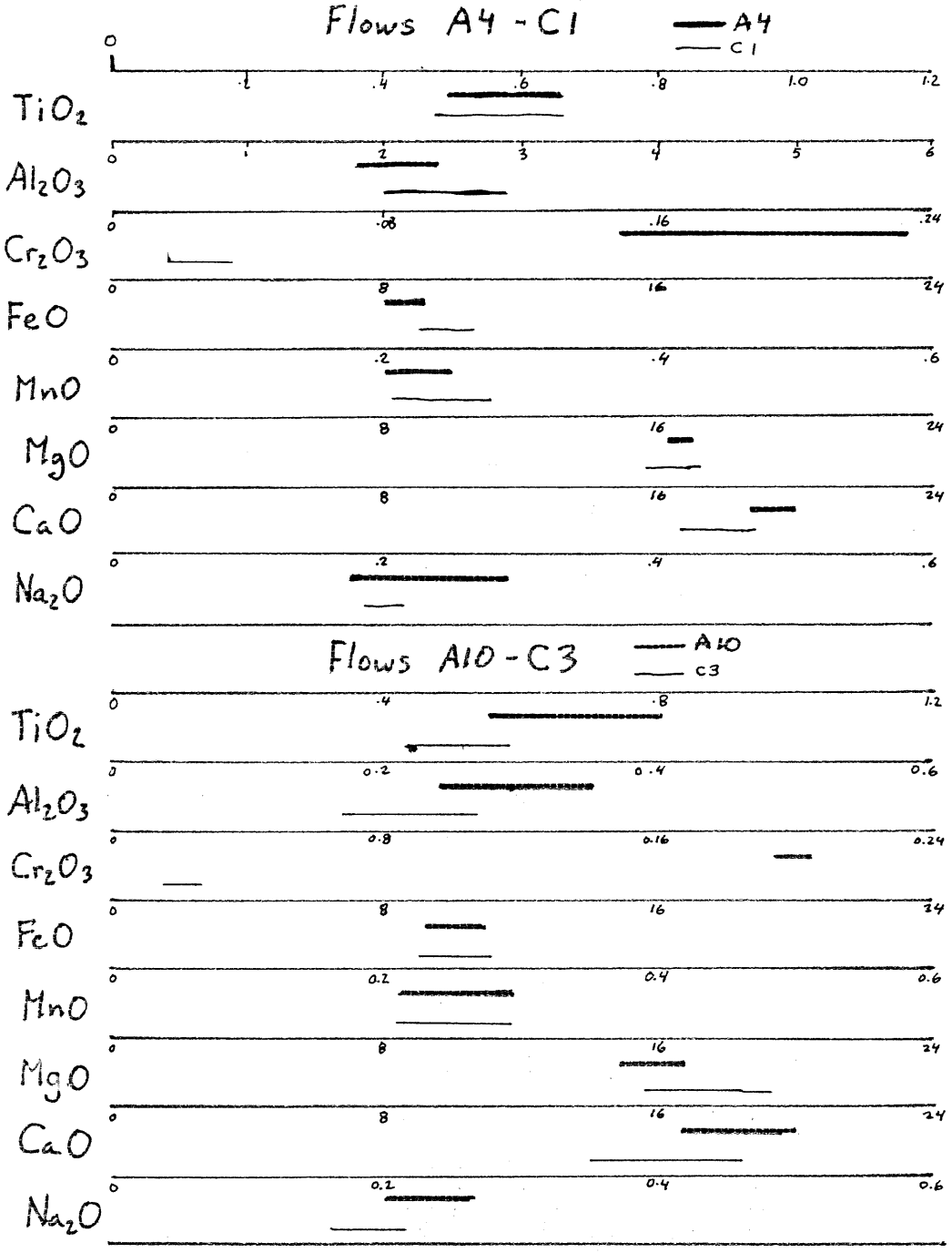


FIGURE 4.1 - Average clinopyroxene compositions for selected samples. The analyses of this study have error bars calculated from the standard deviations. Overlap in the concentrations reduces the reliability of this method of correlation.

correlations should be done on the entire data set. A common technique which treats multivariate data is discriminant analysis. Discriminant analysis uses an extensive reference database to classify different samples into distinct compositional groups. Such a database is not available for the basalts in this area.

An alternative approach never attempted before is to use graphical icons for flow comparison. Each variable in the data set is assigned an icon feature and the final appearance of the icon is a sum of all the variables. Similarities and differences between the data sets are recognized through visual inspection.

Chernoff (1973) introduced a multivariate statistical analysis based on cartoon face icons. He proposed that faces are easy to visualize and remember for correlation. The theory involves the easy integration of several parameters into a unified image within the human mind (Jacob 1983). It is more difficult to obtain a mental image for comparison from other icons such as polygons, trees and castles (Wainer 1983).

Figure 4.2 presents the Chernoff's faces for each flow in the sections of this study. This presentation allows the simultaneous visualization of 14 major and trace element parameters. The faces are created in the ICON option of the computer program SYGRAPH (Wilkinson 1988). Before generating the faces, the different wt% and ppm scales of the elements were standardized to the same scale to prevent distortion of a

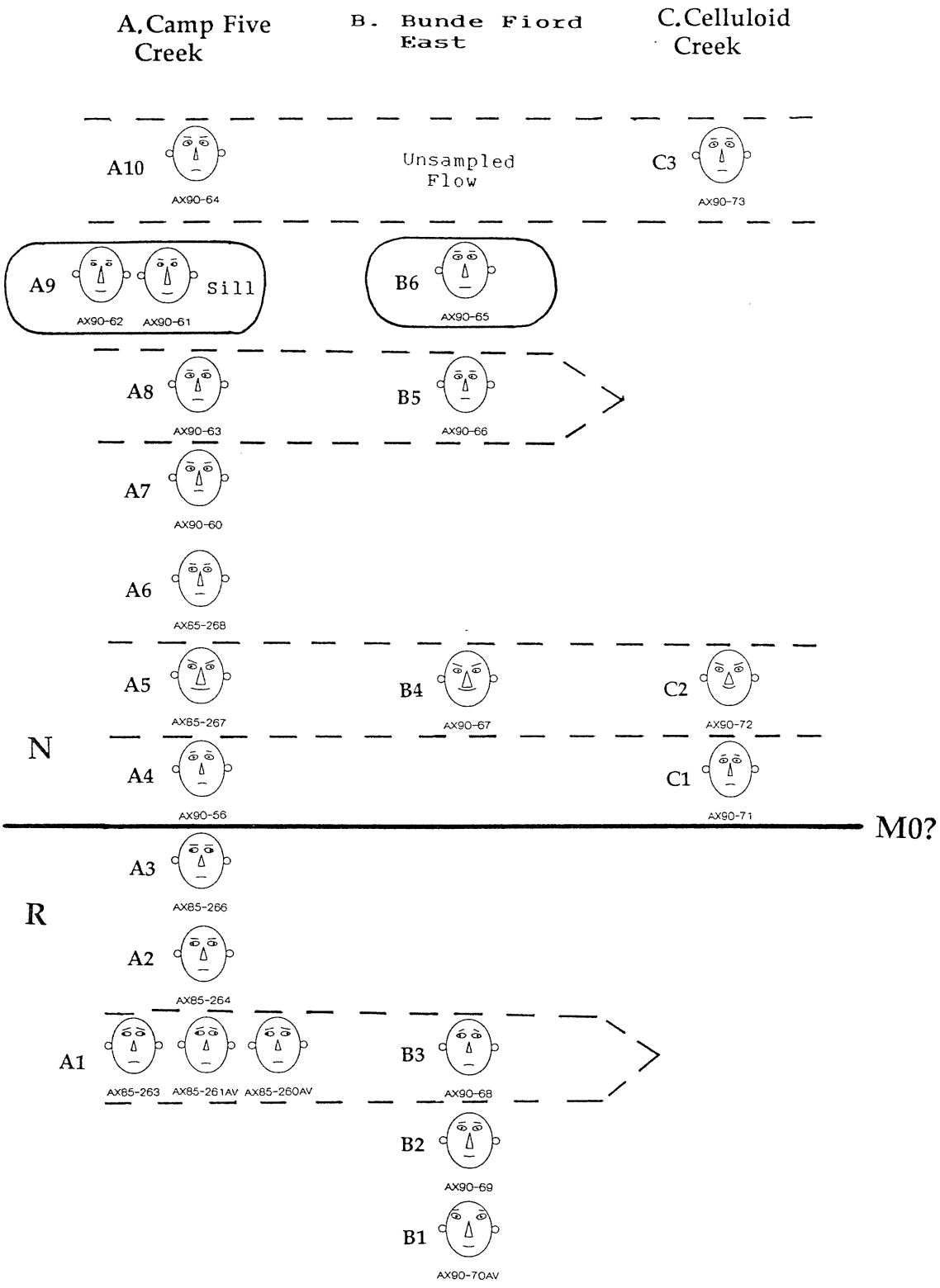


FIGURE 4.2 - The Chernoff icons for the study area basalts. Correlations are made from similar icons. AX90 samples are from this study and AX85 samples are from Williamson (1988). Repeat samples are averaged (AV)

single feature (e.g. the nose) on the face (Wilkinson 1988).

One of the chief criticisms against icons is the assignment order of the data variables to the different parameters of the icon. Opponents of icons argue that false conclusions can result from a random assignment of variables (Jacob 1983). To overcome this, the variables were seriated calculating loadings of the first principal component analysis. Table 4.2 summarizes the organized data and the icon feature assignments. The ordered data of Table 4.2 summarizes the decreasing relationships that each element

Table 4.2 - Parameters for Chernoff's Faces

| | First Prin. Comp. Loadings | Element | Facial Feature |
|---|---|---|---|
| 1 | 0.864 | $P_2O_5$ | Curvature of mouth |
| 2 | 0.836 | Y | Angle of brow |
| 3 | 0.815 | Zr | Width of nose |
| 4 | 0.790 | V | Length of nose |
| 5 | 0.755 | Nb | Length of mouth |
| 6 | -0.703 | Ni | Height of centre of mouth |
| 7 | 0.685 | Zn | Separation of eyes |
| 8 | -0.685 | Cr | Height of centre of eyes |
| 9 | 0.619 | $TiO_2$ | Slant of eyes |
| 10 | 0.580 | $Fe_2O_3$ | Eccentricity of eyes |
| 11 | -0.559 | MgO | Half-length of eyes |
| 12 | 0.429 | Cu | Position of pupils |
| 13 | 0.336 | Ga | Height of eyebrows |
| 14 | 0.226 | Ba | Length of brow |

has to each other. Phosphorus and the incompatible trace elements have the strongest relationships to each other.

To test the reproducibility of Chernoff's faces, multiple samples were analyzed from sill A9 and flow A1. At these locations, the faces for samples from the same unit are virtually identical but retain differences from the overlying and underlying flows not detected by conventional methods. The above test establishes that icons are a valid tool in the correlation of chemically similar basalts.

Many of the icons in the central portion of the three sections are similar and this further substantiates the comagmatic development of these basalts (Figure 4.2). However, subtle differences in the facial expressions allow tentative correlations in this problem area.

In Figure 4.2, sample pairs A5-B4 and A10-C3 have distinct similarities and this reinforces the previous field, petrographic, and geochemical correlations at these locations. Flow C1 and A4 share the same trace element characteristics. Another observation from Figure 4.2 is the distinct similarity between A5, B4, and C2. With exception of the Y-Zr plot, C2 could not be correlated to A5 and B4 with conventional trace element plots. The only difference between C2 and the others is the concentration of Nb (length of mouth). Since all other evidence indicate a strong correlation the analytical value for this element should be re-examined.

Immediately above A5-B4-C3, the chemistry becomes relatively uniform and positive correlations are increasingly difficult. However, A8 and B5 have the closest facial and petrographic resemblances. As well, A6 and A7 have common acicular and lath shaped augites which do not occur in B5 and B6. This petrographic constraint is weak. B5 cannot correlate with A10 and B3 because of the geochemical differences in the Chapter 3 trace element plots. B6 has distinct features and this flow probably pinches out. The two bottom flows of the Bunde Fiord East section have unique icons but the uppermost reversely magnetized B3 floe is similar to the lowermost reversely magnetized flow A1 at Camp Five Creek. This similarity could not be recognized in conventional trace element plots but was suspected in the field (vesiculation pipes). Table 4.3 summarizes the final correlations and Figure 4.3 presents the Walker Island Member stratigraphic profile of the Bunde Fiord area.

**4.6 Summary**

Conventional geochemical and petrographic methods can only successfully correlate two flow pairs (A10-C3 and A5-B4). To complete the correlation, the concentrations of 14 major and trace elements were used and standardized to generate multivariate icons known as Chernoff's faces. Comparison of the icons for each section allows the matching of important flows in problem areas of each section. Some previous petrographic and field comparisons are in error (eg. A8-C1).

Table 4.3 - Final Correlations

| Magnetic Polarity | Flow Number | A Camp Five Ck. | B Bunde Fiord East | C Celluloid Ck. |
|---|---|---|---|---|
| Normal | A10-C3<br><br>B? | - icons<br>- geochem<br>- field match | flow not sampled | - icons<br>- geochem<br>- field match |
| | B6 | XXX | present | XXX |
| | A9 | Sill | XXX | XXX |
| | A8-B5 | - icons<br>- petrography | - icons<br>- petrography | XXX |
| | A7 | present | XXX | XXX |
| | A6 | present | XXX | XXX |
| | A5-B4-C2 | - icons<br>- petrography | - icons<br>- petrography | - icons<br>- petrography |
| | A4-C1 | - icons | XXX | - icons |
| Reverse | A3 | present | XXX | XXX |
| | A2 | present | XXX | XXX |
| | A1-B3 | - petrography<br>- field obs.<br>- icons | - petrography<br>- field obs.<br>- icons | XXX |
| | B2 | XXX | present | XXX |
| | B1 | XXX | present | XXX |

XXX - not present

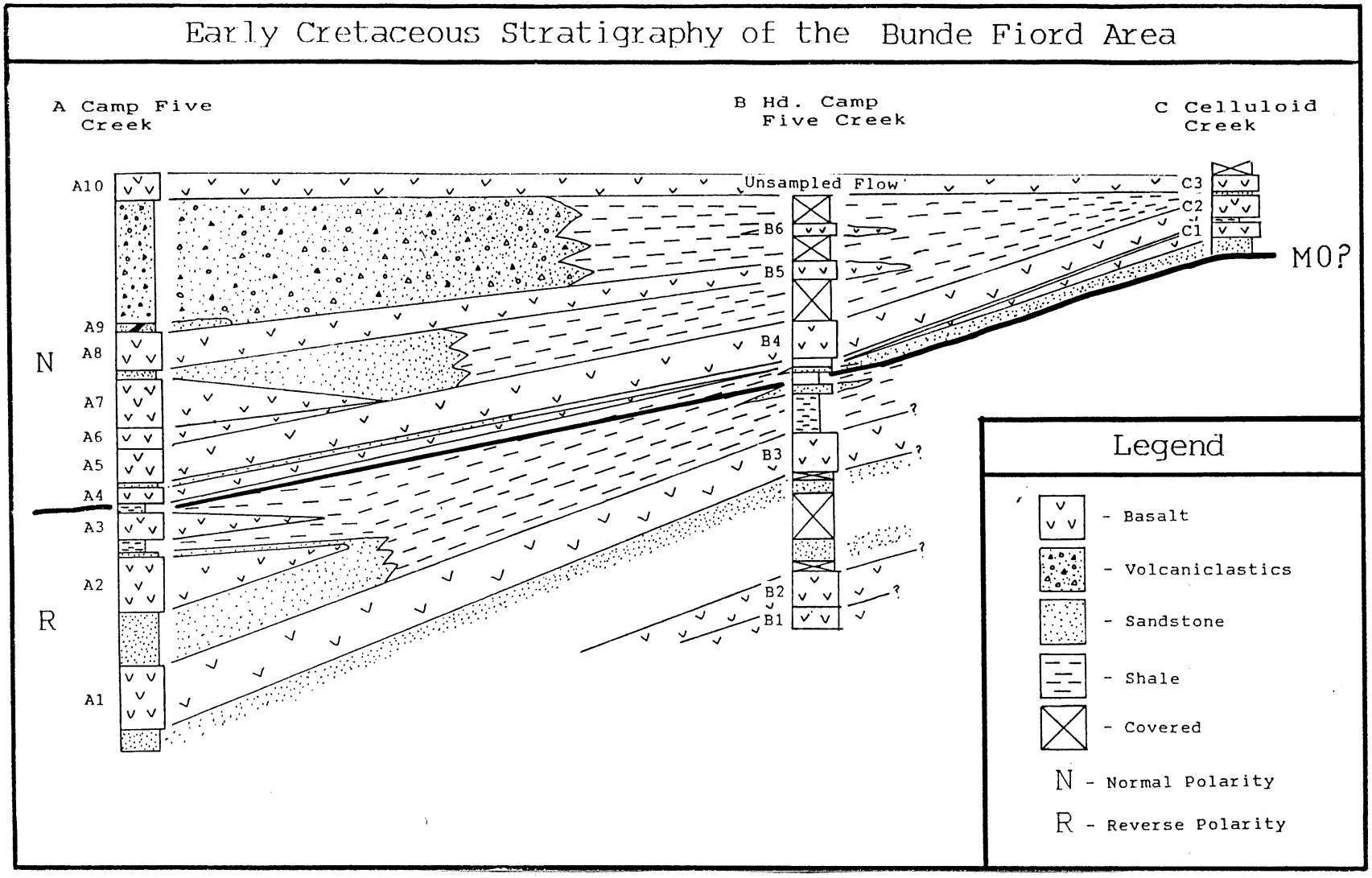


FIGURE 4.3 - Walker Island Member stratigraphy of the Bunde Fiord area

If these correlations are valid, then only one reversal is present in the study area and not two as previously thought (Wynne et al. 1988) . This reversal is probably M0 because all overlying (e.g. Strand Fiord Formation) volcanics and sediments are normally magnetized and may represent the quiet zone.

# CHAPTER 5 - RADIOMETRIC AGE OF THE WALKER ISLAND BASALTS

## 5.1 Introduction

This chapter summarizes the $^{40}Ar/^{39}Ar$ whole-rock age determination results for two flow samples in the Walker Island Member. This is the first radiometric study in this area and the results could be expected to constrain interpretations of the age the Walker Island Group deposition. Only a minimum age estimate is possible for M0 because the two flows chosen for age dating are located above M0 in the stratigraphic section.

## 5.2 The $^{40}Ar/^{39}Ar$ Age Estimation

### 5.2.1 Potassium Distribution

In a $^{40}Ar/^{39}Ar$ analysis of whole-rock samples, the argon release pattern is governed by the mineral phases in which both the radiogenic argon and parent potassium reside. The phenocryst phases of the Walker Island Member basalts only contain minor quantities of potassium in the crystal lattices (Appendix 5). Therefore, the potassium of the basalts is concentrated within the original abundant (up to 20 modal%) interstitial glasses during cooling. Flow C2 has the highest whole-rock potash content ($K_2O$=0.98%) of all the analyzed basalts and contains about 20% of glass alteration products. This is the primary reason for the selection of this sample for the radiogenic analysis. A6 is the freshest sample (rare relict glass) but contains a lower concentration ($K_2O$=0.37%)

of potash.

Volcanic glass is one of the first phases to break down during alteration of basalts. As previously mentioned, the basalts of the study area exhibit minor alteration products. Petrographic analysis of the A6 glass pods reveals isotropic chlorite masses. By comparison, the glass in C2 has been recrystallized to fine grained anhydrous alteration products consisting of potassium feldspar, quartz, and iron oxides. Glasses with chloritic and clay alteration generally yield a lower, false $^{40}Ar/^{39}Ar$ age (McDougall and Harrison 1988). The plot of Figure 3.4 in Chapter 3 indicates re-mobilization of the potassium during alteration.

### 5.2.2 $^{40}Ar/^{39}Ar$ Analyses

Appendix 6 presents a summary of the $^{40}Ar/^{39}Ar$ procedure. The argon release plot for C2 shows an excellent plateau age of 93 Ma for over 90% of $^{39}Ar$ released during the step heating procedure. The plot for A6 has a disturbed appearance which complicates the age estimation. The apparent age decrease from 450-650° could be the result of the outgassing of chlorite and clay alteration products in the glasses (Appendix 6 and Fig. 5.1). These phases have poor argon retention and cannot provide an estimation of extrusive age (Reynolds pers. comm.). In general, the A6 plot produces a 46% $^{39}Ar$ release plateau that yields an age of 89 Ma. This amount is slightly lower than the 50% minimum requirement for a reliable argon degassing plateau (McDougall and Harrison

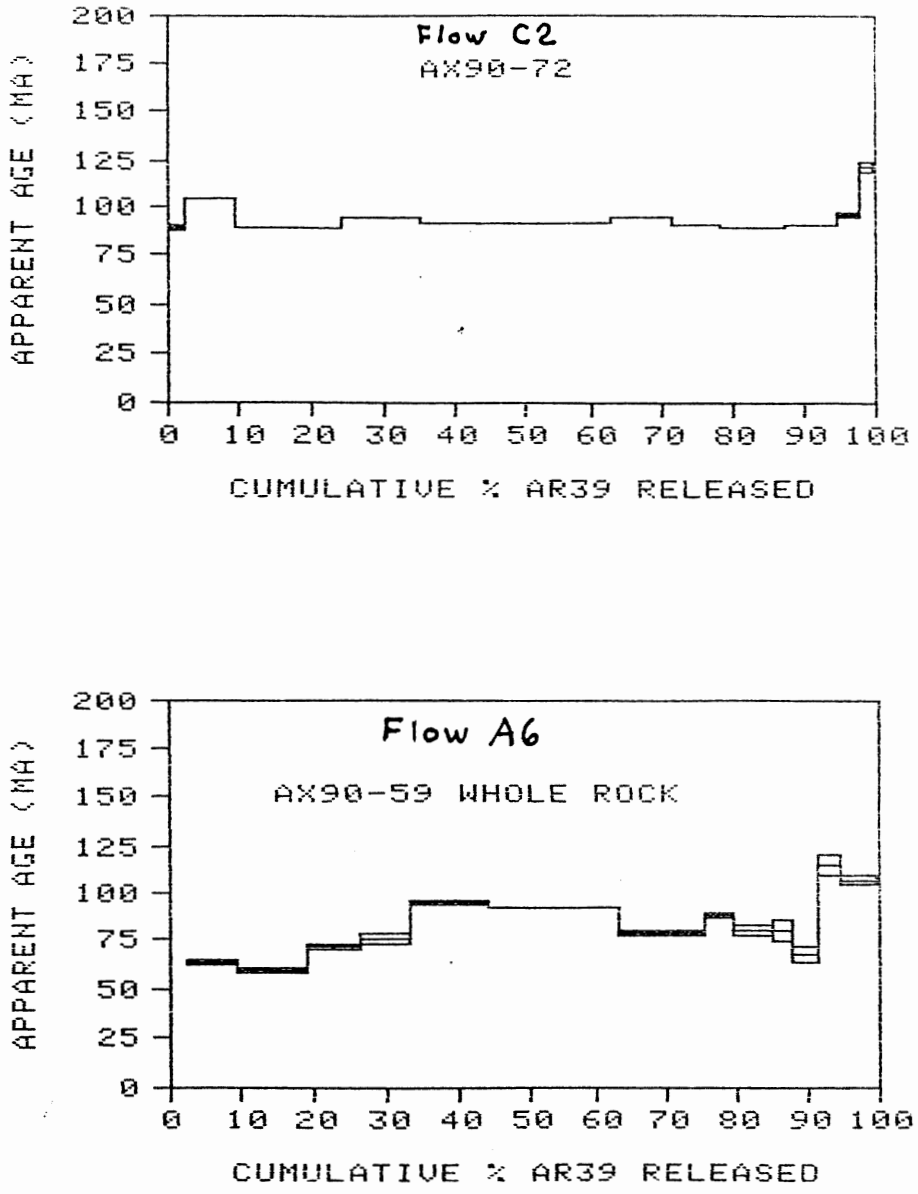


FIGURE 5.1 - The argon degassing plots for A6 and C2.

1988). The two ages are in agreement with each other within the errors of the method.

## 5.3 Interpretation of Results

The 89 and 93 Ma apparent ages of A6 and C2, respectively, would place the basalts within the Late Cenomanian. If these $^{40}Ar/^{39}Ar$ ages represent basalt crystallization, then these dates differ substantially from the stratigraphic and paleontologic ages of the Walker Island Member determined from previous studies (Wynne et al. 1988, Embry and Osadetz 1988). Their paleontological age estimates of sedimentary rocks above and below the Walker Island member basalts constrain it to a Late Barremian-Aptian age of eruption.

There is the remote possibility that the sections were improperly identified since the argon dates are close to the eruption ages of the Strand Fiord basalts. However, extensive field evidence clearly separates the Isachsen and Strand Fiord formations. At Celluloid Creek, flows C1-C3 are overlain by a complete section of recessive Christopher shales which in turn are overlain by an 800+ m section of Strand Fiord basalts. All of the sections have recessive intervals at the top which can only be the Christopher Shales below the Strand Fiord Formation. Also, the Strand Fiord formation erupted during the 40 Ma Cretaceous quiet interval and all basalts have normal magnetic polarity (Wynne et al. 1988). The thick sequence of basalts over C1-C3 at Celluloid Creek all have

normal magnetic polarity (Wynne et al. 1988). The presence of a reversal in the study area basalts distinguishes them from the Strand Fiord formation. Some questionable short term reversals known as the mixed zone occur within the quiet zone (Kent and Gradstein 1986). However, the > 10 m of sediments between the reverse polarity basalts of the A section supports the longevity of the reversal and makes it an unlikely candidate for the mixed zone.

Another possibility is that C2 and A6 could represent younger intrusives (sills) associated with the Strand Fiord formation. Figure 3.2 presents two immobile trace element plots containing the average compositional ratios of both the Strand and Isachsen formations. The bivariate ellipses centre (+/-2 standard deviations) on the mean ratios for the two formations (Williamson 1988, this study). The average Strand Fiord formation ratios were calculated from the Celluloid Creek (N=8) and Artharber Creek (N=11) sections on Bunde Fiord (Williamson 1988). The standard deviations were derived from the analytical precision of the elements under consideration as determined at the XRF at Saint Mary's University. The ellipses have a confidence region of 92.5%.

In the plots, C2 does not display a clear affinity to either the Strand Fiord or the majority of the Isachsen basalts. Therefore, a geochemical comparison does not prove or disprove the hypothesis that the dated samples are younger sills. However, one of the major petrographic features of

A4-B5-C1 is the high (15-20%) content of glass in the unit. Sills usually have a longer rate of cooling which crystallizes the glass depending on the depth of intrusion. Other evidence for the extrusive nature of this unit is the presence of an upright tree stump (rooted) in the top of A5. Immediately overlying C1 is a coal horizon which suggests that the unit (A5-B4-C1) extruded onto the surface and was then subject to a swampy-forest environment. Both petrographic and field observations point to an extrusive origin for this unit.

Alternatively, the radiogenic clock of the basalts could have been reset by a later thermal event after eruption and burial. A re-examination of the C2 glasses provides the answer to the anomalous date. Petrographic studies confirm the presence of low birefringence quartz and K-feldspars among the acicular and dendritic oxides. A very fine coating of oxide dust almost obscures the quartz and K-feldspar. Also, electron microprobe analyses revealed a large K concentration variation across the altered glass pods as the beam moved across a combination of quartz and K-feldspars (Appendix 5). A minor amount of these glass alteration products occurs in A6, but were not analyzed with the electron microprobe.

Unit C2 exhibits little evidence of hydrous chlorite or clay alteration in the crystallized glasses, and hence, aqueous fluids were absent during alteration. The only process which affected the C2 glasses is crystallization. By contrast, the glass in A6 was altered to chloritic material.

The intrusive activity associated with the eruption of 800+ metres of the Strand Fiord Formation probably caused a reheating in the underlying Isachsen basalts. This thermal event, associated with the intrusives, caused the re-mobilization of the potassium in the basaltic glasses. As a result, the $^{40}Ar/^{39}Ar$ procedure provides the date of the recrystallization event and not of the eruption of the Isachsen Formation basalts. The $^{39}Ar$ degassing plateau of Figure 5.1a is a result of K-feldspar since most of the potassium is restricted to the areas of crystallized glass. The less retentive alteration phases in A6 yield a more tentative plateau at 89 Ma.

**5.3 Summary**

The $^{40}Ar/^{39}Ar$ age analysis determines an age (89-93 Ma) for the Isachsen Formation basalts which conflicts with previous paleontological and stratigraphic age estimates. Both geochemical and petrographic studies indicate re-mobilization of potassium initially in the interstitial glass to a retentive potassium-rich feldspar during alteration of C2 which yields an excellent plateau age of 93 Ma. In A6, poorly retentive (hydrous glass alteration) products provide a very tentative age of 89 Ma. As a result, a minimum age cannot be assigned to the M0 reversal in the study area. However, the presence of a high potassium phase in C2 provides an excellent plateau age that may represent the age of the Strand Fiord igneous event - the first such age in the Bunde Fiord area.

# CHAPTER 6 - CONCLUSIONS

## 6.1 Conclusions

A re-examination of the Walker Island Member basalt units changes the previous interpretations of the Early Cretaceous stratigraphy in the Bunde Fiord area of Axel Heiberg Island. Correlation of these units is complicated due to the similar chemical properties of the successive basalt flows in each of the three sections. Ratios of immobile trace elements establish the similarity of two distinct flows and the use of multivariate statistical icons (Chernoff's Faces) provide a more detailed profile of the chemical properties of each flow to complete the correlation. The new petrologic, geochemical, stratigraphic, and $^{40}Ar/^{39}Ar$ analytical data of the study area allow the following conclusions:

1) All basalts of the Walker Island Member are tholeiitic basalts with within-plate to N-type MORB characteristics.

2) Ratios of incompatible trace elements indicate that the Bunde Fiord area was subject to the influence of three distinct magma sources during the Early Cretaceous eruption of the basalts.

3) The distinctive incompatible trace element ratios of two of the flows permit their correlation across the sample area. These correlations are substantiated by stratigraphy, magnetic polarity, and petrology of the basalts.

4) Multivariate analysis allows the additional correlation of flows in the comagmatic suite which could not be compared by trace element ratios.

5) The correlation between the three sections (this study) show that only one magnetic reversal (M0) occurs in the basalt units of the Walker Island Member and not two as previously thought (Wynne et al., 1988).

6) The Celluloid Creek section was erupted at the same time as the lowermost magnetically normal basalts at Camp Five Creek and Bunde Fiord East. This makes them much older than previously interpreted.

7) The Walker Island Group basalts do not have phenocryst phases which accommodate substantial concentrations of potassium. The potassium in the interstitial glasses has been re-mobilized to form either anhydrous K-feldspar bearing assemblages or hydrous secondary clays and chlorites. Hence, an age determination for M0 is impossible under these conditions.

8) The $^{40}Ar/^{39}Ar$ age analysis records the crystallization of the Walker Island Member basalt glasses caused by a thermal event at 89-93 Ma (Late Cenomanian).

9) Intrusive activity associated with the eruption of the Late Albian to Early Cenomanian (800+ m) Strand Fiord basalts could be the cause of the thermal disturbance that reset the Walker Island Member basalt ages.

## REFERENCES

Armstrong RL (1978) Pre-Cenozoic Phanerozoic time scale - computer file of critical dates and consequences of new and in-progress decay-constant revisions. In: Contributions to the geologic time scale. Cohee G, Glaessner M, Hedberg H (eds) AAPG, Tulsa, Okla., pp 73-91

Cameron BI (1989) Petrochemistry and origin of altered Permian basalts in the Sverdrup Basin, Arctic Canada. MSc thesis, Dalhousie University, Halifax, Nova Scotia

Chernoff H (1973) The use of faces to represent points in k-dimensional space graphically. J Amer Statist Assoc 68:361-368

Deer WA, Howie RA, Zussman J (1985) An introduction to the rock forming minerals. Longman Group Ltd, England

Embry AF, Osadetz KG (1988) Stratigraphy and tectonic significance of Cretaceous volcanism in the Queen Elizabeth Islands, Canadian Arctic Archipelago. Can J Earth Sci 25:1209-1219

Hess PC (1989) Origins of igneous rocks. Harvard University Press, London, England,

Huppert HE, Sparks RS (1985) Cooling and contamination of mafic and ultramafic magmas during ascent through continental crust. Earth Planet Sci Lett 74:371-386

Jackson HR, Forsyth DA, Johnson GL (1986) Oceanic affinities of the Alpha Ridge, Arctic Ocean. Mar Geol 73:237-261

Jacob RJ (1983) Investigating the space of Chernoff's faces. In: Recent advances in statistics: papers in honour of Herman Chernoff on his sixtieth birthday. Rizvi MH, Rustagi J, Siegmund D (eds) Academic Press, New York, USA, pp 449-468

Kent DV, Gradstein FM (1986) A Jurassic to recent geochronology. In: The geology of North America, vol. M the western North Atlantic region. Vogt PR, Tucholke BE (eds) Geological Society of America, Boulder, Colorado, pp 45-50

## REFERENCES

Larsen RL, Hilde TW (1975) A revised time scale of magnetic anomalies for the Early Cretaceous and Late Jurassic. J Geophys Res 83: pp 3627-3644

Le Bas MJ, LeMaitre RW, Streckeisen A, Zanettin B (1986) A chemical classification of volcanic rocks based on the total alkali-silica diagram. Jour of Petrol 27: pp 745-750

MacDonald GA, Katsura T (1964) Chemical composition of Hawaiin lavas. Jour of Petrol 5:82-133.

MacKenzie WS, Donaldson CH, Guilford C (1984) Atlas of igneous rocks and their textures. Longman Group Ltd, Essex, England

McDougall I, Harrison TM (1988) Geochronology and thermochronology by the $^{40}Ar/^{39}Ar$ method. Oxford University Press, Oxford England 212p.

Merrett DC, Muecke GK (1989) Preliminary observations on the volcanics of Phillips Inlet, Ellesmere Island: the last phase of Cretaceous volcanism in the Sverdrup Basin.

Meschede M (1986) A method of discriminating between different types of mid ocean ridge basalts and continental tholeiites with the Nb-Zr-Y diagram. Chem Geol 56:207-218

Muecke (1990) Secular and spatial evolution of extensional basin magmatism: development of the Sverdrup Basin, Canadian Arctic Islands. Int Volcanological Congress, Mainz, Federal Republic of Germany, Abstracts, pp 74

Mutter JC, Buck WR, Zehnder CM (1988) Convective partial melting 1. A model for the formation of thick basaltic sequences during the initiation of spreading. J Geophys Res 93:1031-1048

Ogg JG (1987) Magnetostratigraphy of Upper Jurassic and Lower Cretaceous sediments. DSDP site 534, Western North Atlantic. In: Initial reports of the deep sea drilling project, vol. 76. Sherridan RE and others (eds) Washington, USA, pp 685-697

## REFERENCES

Ozima M, Kaneoka I, Yanagisawa M (1978) $^{40}Ar/^{39}Ar$ geochronological studies of drilled basalts from leg 51 and 52. In: Initial reports of the deep sea drilling project, vol. 51,52,53, Donnelly T, Francheteau J, Robinson P, Flower M, Salisbury M (eds) Washington, USA, pp1127-1128

Pearce JA, Cann JR (1973) Tectonic setting of basic volcanic rocks determined using trace element analysis. Earth Planet Sci Lett 19:290-300

Pearce JA, Norry MJ (1979) Petrogenetic implications of Ti, Zr, Y, and Nb variations in volcanic rocks. Contrib Mineral Petrol 69:33-47

Ritcey DH (1989) A geochemical study of the Carboniferous Audhild volcanics, northwestern Ellesmere Island, Atlantic Canada: initial volcanism in the Sverdrup Basin. BSc thesis, Dalhousie University, Halifax, Nova Scotia

Stephenson RA, Embry AF, Nakiboglu SM, Hastaoglu MA (1987) Rift-initiated Permian to Early Cretaceous subsidence of the Sverdrup Basin. In: Sedimentary basins and basin forming processes. Beaumont C, Tankard AJ (eds) Canadian Society of Petroleum Geologists Memoir 12, pp 213-231

Taylor SR, McLennan SM (1985) The continental crust: its composition and evolution. Blackwell Scientific Publications, Oxford, England.

Thorpe RS, Brown GC (1985) The field description of igneous rocks. Open University Press.

Trettin (1989) The arctic islands. In: The geology of North America- an overview. Bally AW, Palmer AR (eds) Boulder, Colorado, pp 349-370

Wainer H (1983) On multivariate display. In: Recent advances in statistics: papers in honour of Herman Chernoff on his sixtieth birthday. Rizvi MH, Rustagi J, Siegmund D (eds) Academic Press, New York, USA, pp 469-508

Wilkinson L (1988) SYGRAPH. SYSTAT Inc. Evanston Ill

## REFERENCES

Williamson MC, (1988) The Cretaceous igneous province of the Sverdrup Basin, Canadian Arctic: field relations and petrochemical studies. PhD Thesis, Dalhousie University, Halifax, Nova Scotia

Williamson MC, Muecke GK (1989) Petrology of igneous rocks from the east-central Sverdrup Basin, Canadian Arctic Archipelago. GAC-MAC Annual meeting, program with abstracts, 14:A96.

Wilson M (1989) Igneous petrogenesis: a global tectonic approach. Unwin Hyman.

Winchester JA, Floyd PA (1977) Geochemical discrimination of different magma series and their products using immobile elements. Chem Geol 20:325-343.

Wynne PJ, Irving E, Osadetz KG (1988) Palaeomagnetism of Cretaceous volcanic rocks of the Sverdrup Basin - magnetostratigraphy, paleolatitudes, and rotations. Can J Earth Sci 25:1220-1239

# APPENDIX 1 - Petrographic Descriptions

## A - Camp Five Creek:

### AX90-56 (A4):

**Phenocrysts:** Glomerophyric and porphyritic (1-3 mm; pl, pl+cpx, pl+ol+cpx, cpx) non-seriate. Plagioclase (45%; .5-3 mm), augite (30%; .5-1 mm), pseudo-olivine (2%; .5-1 mm). Some clusters have up to 20 crystals of both pl and cpx. Individual cpx clusters have about 8 to 16 grains. In general, pl and ol are mostly subhedral, and cpx is subhedral to anhedral. Most pl blocks and laths have oscillatory zoning. **Inclusions:** Some cpx blocks exhibit near-rim inclusion trails. Some pl has core inclusions. **Groundmass:** Hypocrystalline (.1-.3 mm); pl laths, granule cpx-ol, interstitial glass (15%), subhedral oxides (ox; 8%), one amygdule observed ( 1 mm). **Alteration:** Both pl and cpx are fresh with slight edge resorption. The ol and glass are altered to brownish clays and the groundmass pl laths are oriented around the clay filled amygdule. Rare chocolate brown glass with intergrown acicular oxides.

### AX90-57 (A3):

**Phenocrysts:** Glomerophyric to porphyritic (.5-1.5 mm; pl, pl+cpx, cpx) seriate. Plagioclase (50%; .5-1 mm), augite (20%; .5-1mm). All phenocrysts exist alone but are mostly in clusters. Most of the clusters have about 6 cpx and 12 pl grains. The cpx clusters have 6 to 8 grains. Plagioclase is subhedral and cpx-opx are mostly anhedral. One .5mm cpx lath is present. Most of the pl have strong zoning. **Inclusions:** Some inclusions at pl cores but cpx is relatively clear. Some pl clusters are poikilitic at the cores. **Groundmass:** Hypocrystalline (to .3 mm); pl laths, granule cpx, interstitial glass (15%) and carb (5%), subhedral ox (10%), possible late stage elongate ox which cut other crystals. One amygdule observed (.8 mm). **Alteration:** Carbonate replacement in amygdule and in some pl cores. The glass is mostly altered to brownish clays with intergrown acicular ox and the pl exhibits embayment at edges. Some fresh glass is preserved usually in the cores of the glass pods.

A - Camp Five Creek:

**AX90-58 (A5):**

**Phenocrysts:** Glomerophyric (1-2 mm; pl, pl+cpx, pl+ol), non-seriate. Plagioclase (38%; .5-1 mm), augite (32%; .3-1 mm), pseudo-olivine (5%; 1-2 mm). Plagioclase is eu-subhedral while cpx and olivine are sub-anhedral. Pseudo-olivine (some elongate) and pl occur individually but pl is mostly found in clusters. The clusters are usually a combination of about 6 anhedral cpx and 3 pl laths. The rare pl clusters have about 3 pl laths and blocks. almost all cpx exhibit a faint greenish pleochroism. **Inclusions:** Some individual pl gloms are poikilitic near the cores and a few cpx's exhibit inclusion trails plus zoning near the rims. **Groundmass:** Hypocrystalline with trachytoid texture (.15-.5 mm); pl laths; granule cpx-ol, interstitial glass (15%), subhedral ox (10%). Presence of one clay-filled amygdule (1 mm). The glasses are greenish to brown in color. **Alteration:** The pseudomorph olivines are altered to brownish clays. Most phenocrysts are fresh but have irregular edges with little resorption. The groundmass ol has a greenish alteration. Two different types of glasses occur: light brown clay replacement and chocolate-brown devitrification patches with associated elongate oxides. In some areas a blood-red alteration occurs between the glass and oxides (hematite?).

**AX90-59 (A6):**

**Phenocrysts:** Glomerophyric (1-4 mm; 90% pl, pl+cpx), seriate. Plagioclase (35%; 1-4 mm), augite (27%;.5-1 mm). Both pl and cpx are sub-anhedral laths and can occur individually (rare). A typical pl+cpx cluster contains about 3 cpx and 2 pl laths. **Inclusions:** Some larger individual pl and cpx gloms are poikilitic at the cores and some pl+cpx clusters have near-rim inclusions. Some anhedral cpx have near-rim inclusion trails. Most cpx laths (.8-1.0 mm) are inclusion-free but some exhibit near-poikilitic cores. Almost all pl blocks and some pl laths have oscillatory zoning. **Groundmass:** Hypocrystalline (to .1 mm); pl laths, granule cpx, cal (10%), interstitial glass (20%), and subhedral ox (8%). A few amygdules observed (1 mm). The glasses range in color from light to deep brown. **Alteration:** Cals replace some of the groundmass and are at the edges of some amygdules. In one amygdule, cal and clays encircle replacement quartz. Some glass pods are altered into a combination of cal and clays with several elongate oxides. Most of the glasses have chlorite alteration.

A - Camp Five Creek:

**AX90-60 (A7):**

**Phenocrysts:** Glomerophyric (.5-1.5 mm; pl, pl+cpx, pl+ol) seriate. Plagioclase (40%; .5-1 mm), augite (35%; .5-1 mm), pseudomorph olivine (2%; .7 mm). The clusters commonly contain 2 cpx and 1 pl laths. Most pl laths display oscillatory zoning. Besides Plagioclase, cpx occurs as subhedral laths which are mostly acicular. The pseudomorph ol is mostly anhedral. **Inclusions:** Augite exhibits some core inclusions but pl is relatively clean. **Groundmass:** Hypocrystalline (.05-.1 mm); pl laths, granule cpx, ol?, interstitial glass (15%), subhedral ox (10%). Rare amygdules with intruding pl laths. **Alteration:** Most of the pl and cpx have slight edge resorption. Groundmass pl have about 50% edge resorption. The amygdules exhibit clay-chlorite replacement. The glasses are greenish-brown and light-dark chocolate brown. The greenish glasses have clay replacement at pod edges but are fresh at the cores. The darker glasses have associated tiny oxides and resembles AX90-72.

**AX90-61 (A9):**

**Phenocrysts:** Glomerophyric (1-5mm; pl, pl+relict cpx, pl+ol) seriate. Plagioclase (20%; .5-5mm), cpx (0%; .5-.8mm), pseudomorph olivine (2%; .5-1mm). The pl clusters are a combination of 3-4 laths and 1 pseudomorph ol. The relict cpx clusters have 4 anhedral relict cpx and 6-8 pl laths. Preservation of relict cpx zoning. **Inclusions:** Relict cpx has both core and near-rim inclusion trails. Some pl laths exhibit near-core elongate inclusions. Oxides include both phenocrysts and groundmass. **Groundmass:** Hypocrystalline (to .5mm) faint trachytoid texture, pl laths, granule cpx, ox (10%), cal replacement (43%). **Alteration:** Cal, sericite, clay, and chlorite replacement of phenocrysts and groundmass. Some chlorite has replaced the pl lath cores but not exterior. All of the cpx has been replaced with the above secondary products.

## A - Camp Five Creek:

### AX90-62 (A9):

**Phenocrysts:** Glomerophyric (1-5mm; pl, pl+relict cpx, pl+ol) seriate. Plagioclase (20%; .5-5mm), cpx (0%; .5-.8mm), pseudomorph olivine (2%; .5-1mm). The pl clusters are a combination of 3-4 laths and 1 pseudomorph ol. The relict cpx clusters have 4 anhedral relict cpx and 6-8 pl laths. Preservation of relict cpx zoning. **Inclusions:** Relict cpx has both core and near-rim inclusion trails. Some pl laths exhibit near-core elongate inclusions. Oxides include both phenocrysts and groundmass. **Groundmass:** Hypocrystalline, two different sizes (to .3mm and to .5mm). Faint trachytoid texture, pl laths, granule cpx, ox (10%), cal replacement (43%). Presence of clay, cal, and chlorite replacement amygdules (15%; to 3mm). Some amygdules are spherical, others are elongate. **Alteration:** Cal, sericite, clay, and chlorite replacement of phenocrysts and groundmass. Some chlorite has replaced the pl lath cores but not exterior. All of the cpx has been replaced with the above secondary products. Some altered brown glass are present with associated acicular oxides.

### AX90-63 (A8):

**Phenocrysts:** Glomerophyric (1-3 mm; pl, pl+cpx, pl+cpx+ol) mildly seriate. Plagioclase (40%; 1-2 mm), augite (35%; .5-1.5 mm), pseudomorph olivine (10%; 1-3 mm). Plagioclase is subhedral while the cpx and olivines are mostly anhedral. Each phenocryst phase can occur individually. The cpx dominant clusters usually contain about 8 anhedral crystals. Other clusters contain 3 to 6 anhedral cpx and 4 acicular pl. **Inclusions:** Most of the clusters have ox-cpx-pl inclusion at the cores and some individual cpx blocks display two inclusion trails from the core to rim. Some cpxs are poikilitic at the cores. **Groundmass:** Hypocrystalline (.12-.24 mm); pl laths, granule cpx-ol, interstitial glass (10%), subhedral ox (5%). **Alteration:** The ghost olivines are replaced by greenish clays. The cpx and pl have limited resorption. Most groundmass pl exhibit 1/2 edge resorption. Most of the glasses are altered to a greenish or light brown clays but a small amount in the pod centres are fresh. A small amount of chocolate brown glass occurs with intergrown oxides. This glass resembles the glass of AX90-71.

**A - Camp Five Creek:**

**AX90-64 (A10):**

**Phenocrysts:** Glomerophyric (.5 - 2.0 mm; pl+cpx, pl+ol, pl+cpx +ol) non-seriate. Plagioclase (35%; .5-2 mm), augite (30%; .5-1 mm), pseudomorph olivine (15%; .5-1 mm). Typical clusters contain about 4-7 cpx, 2-7 pl, and 1-2 ol. Plagioclase and olivine are eu-subhedral and cpx is mostly sub-anhedral. The subhedral cpx is in the form of laths approximately 1 mm in length. All three phenocryst phases can occur individually. Most pl blocks have oscillatory extinction. **Inclusions:** Both pl and cpx exhibit near rim inclusion trails but pl has core inclusions as well. Some cpx grains have two near-rim inclusion trails while others are near-poikilitic. **Groundmass:** Hypocrystalline (.05-.1 mm), granule pl-cpx-ol, interstitial glass (10%), subhedral ox (10%). Resembles AX90-73 groundmass. One amygdule is observed (1 mm). **Alteration:** Most of the individual pl laths and cpx grains have partial resorption at the edges. The pseudomorph olivines are greenish-brown to brown clay minerals. The glasses range in color from light to dark brown and both types have clay replacement. The amygdule is replaced by a qtz centre surrounded by clays.

**B - Bunde Fiord East:**

**AX90-65 (B6):**

**Phenocrysts:** Glomerophyric (1-5 mm; pl+cpx, pl+cpx+ol+cal) non-seriate. Plagioclase (40%; 1-3 mm), augite (30%; .5-2 mm), pseudomorph olivine (15%; .5-1 mm). Plagioclase and cpx are mostly subhedral. Some cpx and most of the ol are anhedral. All three phenocryst phases can occur individually. Some pl+cpx clusters have greater than 10 grains (2-3 usually cpx). Both pl blocks and laths exhibit oscillatory zoning. **Inclusions:** The subhedral cpx grains have near-rim inclusion trails and other anhedral grains are poikilitic at the cores. Some groundmass pl laths have ox inclusions at the cores. **Groundmass:** hypocrystalline (.04-.1 mm), pl laths, granule cpx-ol, cal (5%), interstitial glass (5%), subhedral ox (5%). **Alteration:** Cal replacement of groundmass and at edges of some clusters. The ol exhibits two different colors of clay replacement: light brown (associated with clusters) and green (individual). The pseudomorph ol grains exhibit albite and qtz replacement cores. As well, the clay replacement glass is greenish in some areas and light brown in others.

B - Bunde Fiord East:

**AX90-66 (B5):**

**Phenocrysts:** Glomerophyric (1-5 mm; pl+cpx), seriate. Plagioclase (35%; 1-4 mm), augite (35%; .5-1.5 mm), pseudomorph olivine (10%; .5-1 mm). The pl clusters have about 12 grains. The cpx clusters have up to 12 anhedral cpx grains intergrown with acicular pl. One observed 2mm cpx lath. The ol is sub-anhedral. Both pl blocks and laths have moderate to strong oscillatory zoning. **Inclusions:** Some pl dominant clusters are poikilitic at the cores and the one cpx lath displays a near-rim inclusion trail. Some cpx grains in the clusters have poikilitic cores. One cpx+pl cluster has near-rim inclusion trails. Other cpx and pl grains are relatively clean. **Groundmass:** Hypocrystalline (.06 mm), pl laths, granule cpx-ol, cal (5%), interstitial glass (10%) subhedral ox (5%). One observed amygdule. **Alteration:** Most smaller pl exhibit 3/4 edge resorption. The cpx have little to no resorption. Cal replacement of groundmass, amygdule, ol, and some glass. In some areas, the glass has altered in the same fashion as AX90-59,71, and 72. The glass is brownish with extensive elongate oxides throughout. The olivines are replaced by greenish clays (iddingsite) and possibly chlorite (faint green pleochroism).

**AX90-67 (B4):**

**Phenocrysts:** Porphyritic to glomerophyric (1-1.5 mm; pl+cpx), seriate. Plagioclase (35%; .5-1 mm), augite (30%; .5-1 mm), pseudomorph olivine (5%; 1mm). Most pl and ol are subhedral. A few cpx are subhedral blocks, but most are anhedral. The pl clusters have 8-9 laths and blocks. The pl+cpx clusters have 6-8 anhedral cpx and 3-4 pl laths. Most of the pl laths and blocks exhibit moderate to strong oscillatory zoning. Almost all cpx have a faint greenish pleochroism. **Inclusions:** Both pl and cpx exhibit core and near-rim inclusion trails as well as rare cpx zoning. Some cpx grains have two inclusion trails. Most clusters have inclusion-rich cores. **Groundmass:** Hypocrystalline with trachytoid texture (.05-.08 mm), pl laths, granule cpx-ol, interstitial glass (20%), subhedral ox (10%). **Alteration:** Both pl and cpx exhibit edge resorption. The ol is replaced by a mixture of chlorite (green pleochroism) and clays. Two different types of glasses occur: light brown clay replacement and chocolate-brown devitrification patches with associated elongate oxides. In some areas a blood-red alteration occurs between the glass and oxides (hematite?).

B - Bunde Fiord East:

**AX90-68 (B3):**

**Phenocrysts:** Glomerophyric (.5-2 mm; pl, pl+cpx, pl+ol), non-seriate. Plagioclase (40%; .5-1.5 mm), augite (34%; .5-1 mm), pseudomorph olivine (1%; .5-1 mm). Most pl and some cpx are subhedral laths with growth twins. Pseudomorph ol, and cpx are mostly anhedral. Some pl+cpx clusters contain 2-3 blocky cpx and 2-3 pl laths. Other pl+cpx clusters have 3 anhedral cpx and a total of 4 pl laths and blocks. The pl clusters contain up to 16 individual laths. All pl has moderate to strong oscillatory zoning. **Inclusions:** Some pl and most cpx display near-rim inclusion trails. Other pl have inclusion-rich cores. Nearly all cpx exhibit near-rim inclusion trails. **Groundmass:** Hypocrystalline (.05-.4 mm), pl laths, granule cpx-ol, cal (10%), interstitial glass (15%), subhedral ox (10%). About 5% amygdules (.5-1.5 mm). **Alteration:** Most pl and cpx are relatively fresh but some display 50% edge resorption. The pseudomorph ol grains are a dark brown clay mineral replacement (chlorophaetite?). The amygdules and glass have mostly cal and clay replacement. Some of the groundmass has cal replacement.

**AX90-69 (B2):**

**Phenocrysts:** Glomerophyric (.5-2 mm; pl, pl+cpx, cpx), non-seriate. Plagioclase (30%; .5-2 mm), augite (30%; .5-.8 mm). Most of the pl and some cpx is subhedral. The cpx is mostly anhedral. Most of the clusters contain 2 anhedral cpxs and 3-4 pl laths. Some pl clusters contain about 8 near-acicular pl laths. Most of the pl clusters have 2-3 1-2mm blocks and 8-10 smaller laths. The pl blocks exhibit strong oscillatory zoning. **Inclusions:** The pl clusters are poikilitic at the cores. Most of the cpx exhibits near-rim inclusion trails. **Groundmass:** Hypocrystalline (.05-.4 mm), pl laths, granule cpx, cal (20%), interstitial glass (5%), subhedral ox (15%). **Alteration:** Most of the pl and cpx edges have resorption. Light brown glasses are completely devitrified into clay crystals. The dark brown glasses are still isotropic at the pod cores. Cal replacement in the groundmass.

## B - Bunde Fiord East:

### AX90-70 (B1):

**Phenocrysts:** Glomerophyric (.5-2 mm; pl, cpx, pl+cpx, pl+ol), non-seriate. Plagioclase (30%; 1-2 mm), augite (29%; mm), pseudomorph olivine (1%; mm). Both pl and minor cpx form laths. Most of the ol and cpx are sub-anhedral. Some cpx and pl occur individually. The pl clusters contain about 12 grains and the cpx clusters have about 8-10 grains. **Inclusions:** Some pl clusters are poikilitic at cores while the pl lath clusters are relatively clear. Most of the cpx have near-rim inclusion trails. Some individual cpxs are poikilitic. **Groundmass:** Hypocrystalline (.05 and .05-.1 mm), pl laths, granule cpx-ol, cal (5%), interstitial glass (15%), subhedral ox (15%). Two grain sizes of groundmass exist. The finer grain groundmass surrounds some of the pl dominant clusters. **Alteration:** Some cpx and pl exhibit edge resorption. Some pseudomorph olivines have cal and qtz alteration. The glass ranges in color from medium-dark to greenish brown. The greenish glass is devitrified into clays and has a few associated elongated opaques. The groundmass pl laths exhibit some edge resorption.

## C - Celluloid Creek:

### AX90-71 (C1):

**Phenocrysts:** Glomerophyric to hypocrystalline (1-4 mm; pl, pl+ol, pl+cpx, cpx), seriate. Plagioclase (30%; .5-3 mm), augite (30%; .5-2 mm), pseudomorph olivine (5%; .5-1 mm). Plagioclase occurs as subhedral laths. Augite, ol and minor pl are mostly anhedral. Olivine can occur individually. Most of the clusters contain 6-8 anhedral cpx and 2-3 acicular pl. The pl clusters contain up to 10 grains. Both pl blocks and laths exhibit strong oscillatory zoning. **Inclusions:** Some of the pl, and pl+cpx clusters have near-poikilitic cores. Most cpx grains and 2 rare laths display poikilitic cores. The remaining clusters are relatively inclusion-free. Some cpx blocks have near-rim inclusion trails. **Groundmass:** Hypocrystalline (.05-.15 mm), pl laths, granule cpx-ol, cal (5%), interstitial glass (20%), subhedral ox (10%). One amygdule observed (1 mm). **Alteration:** Both cpx and pl exhibit minor edge resorption. Clay replacement ol is greenish brown to brown in color. All glass is devitrified into clays and range in color from light to darker greenish brown.

C - Celluloid Creek:

**AX90-72 (C2):**

**Phenocrysts:** Porphyritic with rare Glomerophyric Plagioclase (38%; 1-2 mm; pl), augite (35%; .5-.8 mm), pseudomorph olivine (2%; .5-1 mm), seriate. Only pl occurs as subhedral laths and the individual cpx and ol grains are mostly anhedral. **Inclusions:** The pl cluster and individual pl+cpx grains exhibit near-core inclusions. Some of the smaller (.5 mm) cpx grains have both near-rim inclusion trails and zoning. **Groundmass:** Hypocrystalline (.04-.15 mm), pl laths, granule cpx-ol, interstitial glass (15%), subhedral ox (10%). **Alteration:** All of the glass has devitrified into clays with a lattice of skeletal oxides and pl. Some pl sericite alteration near cores. Most of the pl and cpx have edge resorption. The pseudomorph ol is medium to dark brown clay minerals but some original ol remnants remain near the cores.

**AX90-73 (C3):**

**Phenocrysts:** Glomerophyric (.5-2 mm; pl, pl+cpx, pl+ol), non-seriate. Plagioclase (35%; .5-2 mm), augite (30%; .5-1.5 mm), pseudomorph olivine (15%; .5 mm). Both pl and ol are mostly eu-subhedral and cpx is anhedral (rare zoning). Pseudo-olivine mainly occurs individually. Typical clusters contain about 4-7 cpx, 2-7 pl, and 1-2 ol. **Inclusions:** Most pl exhibit near-core oxide inclusions and some cpxs are almost poikilitic. Other cpx blocks exhibit near-rim inclusions. Some of the groundmass pl have near core inclusions. One amygdule observed (1 mm). **Groundmass:** Hypocrystalline (.02-.06 mm; pl laths, granule cpx-ol, interstitial glass (10%), subhedral ox (10%). **Alteration:** Both pl and cpx have mild to strong edge resorption. Cal replacement in the groundmass. The pseudomorph olivines are mostly greenish brown to brown clay minerals. The glasses are altered to dark brown clays.

# APPENDIX 2 - Whole-Rock Geochemistry

**Methods:**

A total of 16 basalt samples were processed at Dalhousie University. The processing involved cutting and grinding of the sample to remove the weathered surface and rock saw contamination. Next, the sample was pulverized and homogenized into a -100 mesh powder. The 16 sample powders (along with standards and duplicates) were submitted to the X-Ray Fluorescence (XRF) Laboratory at Saint Mary's University. The laboratory staff heated the sample batch to 1050° C for 4 hours. The heating causes the transformation of all ferrous iron ($FeO_2$) into ferric ($Fe_2O_3$) iron and the loss of volatiles such as carbon dioxide and water (loss on ignition). The resultant list of major and trace elements for each sample are on the next pages.

Table 2.1 - Major and Trace Elements
Oxides and Loss on Ignition (wt%)
Trace Elements (ppm)

| | **A1** AX85-261 | **A5** AX85-264 | **A3** AX85-266 | **A4** AX90-56 | **A5** AX85-267 |
|---|---|---|---|---|---|
| $SiO_2$ | 49.00 | 51.24 | 49.76 | 48.83 | 50.99 |
| $Al_2O_3$ | 14.02 | 13.51 | 13.16 | 13.79 | 12.96 |
| $Fe_2O_3$ | 12.08 | 12.63 | 14.24 | 13.38 | 14.31 |
| MgO | 5.63 | 5.69 | 4.89 | 5.50 | 4.57 |
| CaO | 10.75 | 10.09 | 9.94 | 10.66 | 8.77 |
| $Na_2O$ | 2.06 | 2.28 | 2.32 | 2.17 | 2.59 |
| $K_2O$ | 0.23 | 0.34 | 0.74 | 0.14 | 0.68 |
| $TiO_2$ | 2.25 | 2.17 | 2.05 | 1.94 | 2.66 |
| MnO | 0.18 | 0.20 | 0.22 | 0.20 | 0.29 |
| $P_2O_5$ | 0.22 | 0.22 | 0.22 | 0.19 | 0.29 |
| L.O.I. | 2.00 | 2.20 | 4.08 | 1.80 | 2.41 |
| Total | 98.42 | 100.57 | 101.62 | 98.60 | 100.44 |
| Ba | 238.00 | 188.00 | 190.00 | 107.00 | 276.00 |
| Rb | 7.00 | 10.00 | 19.00 | 9.00 | 19.00 |
| Sr | 335.00 | 229.00 | 201.00 | 219.00 | 243.00 |
| Y | 30.00 | 40.00 | 38.00 | 33.00 | 49.00 |
| Zr | 163.00 | 190.00 | 183.00 | 144.00 | 253.00 |
| Nb | 11.00 | 13.00 | 12.00 | 8.00 | 33.00 |
| Th | <10.00 | 1.00 | 0.00 | <10.00 | 3.00 |
| Pb | 11.00 | 9.00 | 8.00 | <10.00 | 8.00 |
| Ga | 25.00 | 20.00 | 18.00 | 23.00 | 17.00 |
| Zn | 100.00 | 114.00 | 106.00 | 107.00 | 119.00 |
| Cu | 157.00 | 133.00 | 125.00 | 197.00 | 147.00 |
| Ni | 77.00 | 58.40 | 40.00 | 54.00 | 25.00 |
| V | 310.00 | 376.00 | 345.00 | 347.00 | 495.00 |
| Cr | 85.00 | 56.00 | 66.00 | 75.00 | 17.00 |

Table 2.1 - Major and Trace Elements
Oxides and Loss on Ignition (wt%)
Trace Elements (ppm)

| | **A6** AX90-268 | **A7** AX90-60 | **A9** AX90-61 | **A9** AX90-62 | **A8** AX90-63 |
|---|---|---|---|---|---|
| $SiO_2$ | 50.83 | 50.48 | 36.56 | 34.97 | 48.38 |
| $Al_2O_3$ | 13.11 | 12.29 | 16.25 | 15.43 | 12.91 |
| $Fe_2O_3$ | 14.31 | 14.56 | 16.76 | 14.15 | 14.11 |
| MgO | 4.86 | 4.98 | 1.91 | 1.77 | 5.33 |
| CaO | 9.77 | 9.58 | 13.53 | 17.03 | 10.83 |
| $Na_2O$ | 2.41 | 2.33 | 2.67 | 2.77 | 2.46 |
| $K_2O$ | 0.36 | 0.28 | 0.16 | 0.17 | 0.18 |
| $TiO_2$ | 2.32 | 2.35 | 2.52 | 2.58 | 2.13 |
| MnO | 0.20 | 0.21 | 0.26 | 0.33 | 0.20 |
| $P_2O_5$ | 0.23 | 0.24 | 0.29 | 0.29 | 0.22 |
| L.O.I. | 2.47 | 1.80 | 10.10 | 12.60 | 1.90 |
| Total | 100.44 | 99.10 | 101.01 | 102.09 | 98.65 |
| Ba | 142.00 | 174.00 | 93.00 | 106.00 | 119.00 |
| Rb | 12.00 | 14.00 | 6.00 | 0.00 | 0.00 |
| Sr | 196.00 | 211.00 | 227.00 | 240.00 | 223.00 |
| Y | 42.00 | 41.00 | 42.00 | 37.00 | 38.00 |
| Zr | 169.00 | 179.00 | 168.00 | 175.00 | 155.00 |
| Nb | 13.00 | 10.00 | 13.00 | 13.00 | 13.00 |
| Th | 0.00 | <10.00 | <10.00 | <10.00 | <10.00 |
| Pb | 6.00 | <10.00 | <10.00 | <10.00 | <10.00 |
| Ga | 20.00 | 24.00 | 28.00 | 24.00 | 19.00 |
| Zn | 107.00 | 121.00 | 112.00 | 123.00 | 112.00 |
| Cu | 156.00 | 220.00 | 241.00 | 249.00 | 223.00 |
| Ni | 33.00 | 40.00 | 68.00 | 61.00 | 54.00 |
| V | 416.00 | 418.00 | 504.00 | 481.00 | 394.00 |
| Cr | 33.00 | 35.00 | 51.00 | 41.00 | 37.00 |

Table 2.1 - Major and Trace Elements
Oxides and Loss on Ignition (wt%)
Trace Elements (ppm)

| | **A10** AX90-64 | **B6** AX90-65 | **B5** AX90-66 | **B4** AX90-67 | **B3** AX90-68 |
|---|---|---|---|---|---|
| $SiO_2$ | 49.25 | 49.06 | 47.84 | 50.48 | 46.72 |
| $Al_2O_3$ | 13.04 | 13.19 | 13.31 | 12.83 | 13.42 |
| $Fe_2O_3$ | 14.74 | 13.57 | 13.84 | 14.19 | 13.03 |
| MgO | 5.35 | 5.56 | 4.69 | 4.30 | 5.48 |
| CaO | 9.89 | 10.89 | 11.09 | 8.79 | 11.52 |
| $Na_2O$ | 2.19 | 2.24 | 2.37 | 2.63 | 1.96 |
| $K_2O$ | 0.48 | 0.37 | 0.22 | 0.58 | 0.16 |
| $TiO_2$ | 1.72 | 2.37 | 2.12 | 2.62 | 2.17 |
| MnO | 0.22 | 0.19 | 0.21 | 0.21 | 0.18 |
| $P_2O_5$ | 0.19 | 0.25 | 0.23 | 0.31 | 0.21 |
| L.O.I. | 1.90 | 1.30 | 2.40 | 2.10 | 4.70 |
| Total | 98.97 | 98.99 | 98.32 | 99.04 | 99.28 |
| Ba | 187.00 | 115.00 | 131.00 | 284.00 | 113.00 |
| Rb | 11.00 | 10.00 | 13.00 | 38.00 | 6.00 |
| Sr | 180.00 | 238.00 | 225.00 | 264.00 | 304.00 |
| Y | 40.00 | 37.00 | 36.00 | 47.00 | 26.00 |
| Zr | 133.00 | 171.00 | 151.00 | 270.00 | 149.00 |
| Nb | 9.00 | 13.00 | 10.00 | 31.00 | 11.00 |
| Th | <10.00 | <10.00 | <10.00 | 10.00 | <10.00 |
| Pb | 12.00 | <10.00 | <10.00 | 11.00 | <10.00 |
| Ga | 24.00 | 21.00 | 23.00 | 29.00 | 22.00 |
| Zn | 111.00 | 100.00 | 107.00 | 127.00 | 103.00 |
| Cu | 217.00 | 217.00 | 215.00 | 215.00 | 142.00 |
| Ni | 64.00 | 66.00 | 49.00 | 28.00 | 71.00 |
| V | 386.00 | 397.00 | 370.00 | 469.00 | 326.00 |
| Cr | 62.00 | 99.00 | 27.00 | 11.00 | 84.00 |

Table 2.1 - Major and Trace Elements
Oxides and Loss on Ignition (wt%)
Trace Elements (ppm)

| | **B2** AX90-69 | **B1** AX90-70 | **C1** AX90-71 | **C2** AX90-72 | **C3** AX90-73 |
|---|---|---|---|---|---|
| $SiO_2$ | 47.96 | 47.32 | 47.33 | 49.72 | 48.87 |
| $Al_2O_3$ | 12.25 | 12.52 | 13.08 | 12.40 | 12.70 |
| $Fe_2O_3$ | 12.68 | 13.97 | 13.54 | 14.53 | 14.64 |
| MgO | 5.76 | 5.89 | 5.23 | 4.70 | 5.44 |
| CaO | 11.08 | 10.05 | 11.99 | 9.21 | 10.36 |
| $Na_2O$ | 2.08 | 2.03 | 2.11 | 2.55 | 2.06 |
| $K_2O$ | 0.23 | 0.15 | 0.14 | 0.98 | 0.43 |
| $TiO_2$ | 2.83 | 2.89 | 1.96 | 2.66 | 1.68 |
| MnO | 0.19 | 0.20 | 0.20 | 0.21 | 0.22 |
| $P_2O_5$ | 0.28 | 0.29 | 0.20 | 0.34 | 0.21 |
| L.O.I. | 3.20 | 3.80 | 4.00 | 0.70 | 1.40 |
| Total | 98.54 | 99.11 | 99.78 | 98.00 | 98.01 |
| Ba | 176.00 | 84.00 | 107.00 | 240.00 | 147.00 |
| Rb | 5.00 | 0.00 | 0.00 | 39.00 | 11.00 |
| Sr | 310.00 | 303.00 | 230.00 | 206.00 | 171.00 |
| Y | 34.00 | 35.00 | 31.00 | 47.00 | 38.00 |
| Zr | 192.00 | 200.00 | 133.00 | 245.00 | 132.00 |
| Nb | 13.00 | 14.00 | 10.00 | 20.00 | 10.00 |
| Th | <10.00 | <10.00 | <10.00 | <10.00 | <10.00 |
| Pb | <10.00 | 10.00 | <10.00 | 14.00 | <10.00 |
| Ga | 25.00 | 28.00 | 21.00 | 21.00 | 19.00 |
| Zn | 101.00 | 153.00 | 99.00 | 129.00 | 113.00 |
| Cu | 188.00 | 203.00 | 190.00 | 177.00 | 205.00 |
| Ni | 56.00 | 64.00 | 53.00 | 31.00 | 55.00 |
| V | 450.00 | 454.00 | 390.00 | 362.00 | 389.00 |
| Cr | 82.00 | 84.00 | 33.00 | 35.00 | 63.00 |

## APPENDIX 3 - Sample Statistics

Analysis of sample duplicates ensure the reproducibility of the data base with the X-Ray fluorescence procedure. Table 3.1 presents statistics of five XRF analyses on flow #1 of Camp Five Creek. Three of the results are from Williamson (1988) and two are duplicate samples from this study. All the important element standard deviations used in this study are lower than the maximum 10% error of the XRF. The statistical analysis enables the comparison of all samples and the construction of accurate element plots for the correlation (Muecke, pers. comm.).

**Table 3.1 - Repeat Sample (A1) Statistics**

| Major Elements (%) | | | Trace Elements (ppm) | | |
|---|---|---|---|---|---|
| Oxide | Mean | Std. dev | Element | Mean | Std. dev |
| $SiO_2$ | 49.45 | 0.39 | Ba | 250.20 | 20.44 |
| $Al_2O_3$ | 14.07 | 0.35 | Cr | 83.40 | 7.12 |
| $Fe_2O_3$ | 12.32 | 0.45 | Sr | 323.80 | 8.93 |
| MgO | 5.68 | 0.22 | Y | 31.20 | 1.79 |
| CaO | 10.64 | 0.48 | Zr | 164.20 | 7.29 |
| $Na_2O$ | 2.28 | 0.13 | Nb | 12.40 | 1.14 |
| $K_2O$ | 0.32 | 0.15 | Ga | 21.60 | 2.30 |
| $TiO_2$ | 2.32 | 0.07 | Zn | 102.40 | 10.01 |
| MnO | 0.19 | 0.01 | Cu | 122.20 | 23.72 |
| $P_2O_5$ | 0.22 | 0.02 | Ni | 70.96 | 6.03 |
| Total | 99.98 | 1.40 | V | 326.40 | 11.46 |

# APPENDIX 4 - Plagioclase and Glass Compositions

The following table summarizes the average plagioclase core compositions for flows A6 and C2.

| Plagioclase Compositions for Flows A6 and C2 | | | | |
|---|---|---|---|---|
| | Flow A6 (n=7) | | Flow C2 (n=10) | |
| Oxide | Mean (%) | Std. Dev | Mean (%) | Std. Dev |
| $SiO_2$ | 49.71 | 1.63 | 55.23 | 0.90 |
| $TiO_2$ | 0.06 | 0.02 | 0.07 | 0.01 |
| $Al_2O_3$ | 30.95 | 1.00 | 27.58 | 0.57 |
| FeO | 0.65 | 0.09 | 0.60 | 0.06 |
| MgO | 0.18 | 0.03 | 0.09 | 0.02 |
| CaO | 14.98 | 1.02 | 10.88 | 0.64 |
| $Na_2O$ | 3.08 | 0.56 | 5.31 | 0.33 |
| $K_2O$ | 0.12 | 0.04 | 0.00 | 0.00 |
| Total | 99.73 | 0.63 | 99.77 | 0.57 |

The table on the next page summarizes the glass compositions for Flows A6 and C2.

| The Glass Compositions of Flows A6 and C2 | | | | | | | | | | |
|---|---|---|---|---|---|---|---|---|---|---|
| Oxide | $SiO_2$ | $TiO_2$ | $Al_2O_3$ | FeO | MnO | MgO | CaO | $Na_2O$ | $K_2O$ | Total |
| Flow A6 | 68.55 | 0.47 | 11.83 | 2.51 | 0.01 | 0.31 | 3.08 | 0.66 | 1.42 | 88.83 |
| | 73.85 | 0.46 | 11.62 | 1.31 | 0.00 | 0.08 | 0.78 | 3.56 | 1.64 | 93.28 |
| | 71.34 | 0.36 | 15.53 | 1.02 | 0.00 | 0.04 | 2.40 | 4.27 | 1.86 | 96.81 |
| | 71.17 | 0.51 | 12.74 | 1.23 | 0.00 | 0.02 | 0.60 | 1.87 | 1.92 | 90.05 |
| | 73.81 | 0.58 | 12.93 | 1.24 | 0.00 | 0.00 | 0.56 | 2.39 | 2.97 | 94.48 |
| | 48.26 | 0.14 | 6.68 | 23.62 | 0.09 | 4.12 | 1.16 | 0.64 | 1.12 | 85.84 |
| | 70.81 | 0.72 | 11.81 | 1.42 | 0.00 | 0.05 | 2.75 | 1.37 | 1.65 | 90.58 |
| | 41.03 | 0.14 | 4.33 | 25.10 | 0.09 | 5.21 | 1.23 | 3.49 | 0.00 | 80.63 |
| | 39.44 | 0.14 | 4.50 | 24.49 | 0.09 | 5.68 | 1.21 | 5.08 | 0.10 | 80.73 |
| | 40.73 | 0.15 | 4.46 | 25.23 | 0.11 | 5.50 | 1.22 | 1.52 | 0.00 | 78.93 |
| | 40.26 | 0.20 | 4.47 | 24.77 | 0.14 | 4.96 | 1.19 | 2.53 | 0.00 | 78.52 |
| | 41.25 | 0.17 | 4.48 | 25.36 | 0.14 | 5.08 | 1.16 | 1.79 | 0.00 | 79.45 |
| | 43.14 | 0.17 | 4.47 | 25.35 | 0.14 | 5.06 | 1.16 | 1.78 | 0.00 | 81.28 |
| | 64.56 | 0.18 | 19.36 | 1.00 | 0.00 | 0.08 | 3.71 | 6.68 | 0.75 | 96.34 |
| | 42.12 | 0.17 | 4.63 | 26.10 | 0.14 | 5.41 | 1.29 | 0.83 | 0.00 | 80.71 |
| | 65.50 | 0.03 | 17.59 | 1.11 | 0.00 | 0.06 | 1.35 | 4.82 | 7.55 | 98.03 |
| | 55.90 | 0.00 | 13.30 | 9.42 | 0.11 | 1.33 | 2.93 | 3.45 | 5.42 | 91.85 |
| Flow C2 | 38.20 | 0.32 | 9.27 | 29.98 | 0.23 | 4.74 | 1.43 | 1.11 | 3.32 | 88.60 |
| | 59.69 | 0.45 | 14.81 | 9.51 | 0.05 | 1.70 | 0.75 | 2.07 | 8.90 | 97.97 |
| | 72.30 | 0.34 | 12.91 | 3.37 | 0.02 | 0.48 | 1.01 | 3.80 | 4.90 | 99.11 |
| | 53.95 | 0.60 | 8.38 | 17.51 | 0.28 | 3.11 | 10.96 | 2.02 | 0.97 | 97.78 |
| | 69.33 | 0.27 | 13.72 | 4.06 | 0.02 | 0.71 | 0.72 | 3.86 | 5.35 | 98.04 |
| | 58.96 | 0.13 | 15.01 | 9.53 | 0.01 | 1.67 | 0.50 | 2.25 | 8.09 | 96.17 |
| | 91.86 | 0.01 | 4.70 | 1.45 | 0.00 | 0.24 | 0.25 | 1.10 | 1.69 | 101.30 |
| | 78.12 | 0.88 | 11.51 | 2.20 | 0.03 | 0.20 | 0.82 | 3.62 | 3.24 | 100.61 |

# APPENDIX 5 - The $^{40}Ar/^{39}Ar$ Analysis

## A1 Procedure

Each basalt sample is ground to a -60 to -80 mesh size and washed with distilled water to eliminate contaminants. The samples are then packaged in a aluminum foil disk and sent to McMaster University. At McMaster, the foil disks and special known standards are irradiated in a nuclear reacter to produce $^{39}Ar$ from $^{39}K$ and $^{40}Ar$ from $^{40}K$. The standards are placed in known positions in the irradiation can in order to compensate for variation in the neutron dose at different levels. The standards provide the concentrations of the flux (i.e. neutron concentration) which is the major parameter in the constant J.

At Dalhousie, the samples are put in a furnace and heated in a series of steps in order to release the Ar. At the end of each step, the amount of $^{40}Ar$ and $^{39}Ar$ is measured in the mass spectrometer and then incorporated into the following equation:

$$t\ (age) = \frac{1}{L} * \log \left[ 1 + \frac{^{40}Ar}{^{39}Ar} * J \right]$$

$$L\ (decay\ constant) = 5.544 * 10^{-10}\ /yr$$

Summaries of the step age determinations for flows A6 and C2 are on the next two pages.

# AX90-59 WHOLE ROCK SUMMARY

(A6)

| °C | mV 39 | % 39 | AGE(Ma) | % ATMOS | 37/39 | 40/36 | 39/36 | % IIC |
|---|---|---|---|---|---|---|---|---|
| 450 | 5 | 3 | -47 +/- 1 | 119 | 2.245 | 248 | 4.292 | 1 |
| 500 | 13 | 7 | 64 +/- 3 | 69 | 2.357 | 426 | 8.466 | 1 |
| 550 | 18 | 10 | 59 +/- 2 | 63 | 3.844 | 470 | 12.151 | 2 |
| 600 | 14 | 7 | 71 +/- 2 | 60 | 6.399 | 489 | 11.228 | 3 |
| 650 | 13 | 7 | 76 +/- 3 | 68 | 8.477 | 436 | 7.644 | 4 |
| 700 | 21 | 11 | 95 +/- 2 | 49 | 9.553 | 606 | 13.415 | 4 |
| 750 | 36 | 19 | 92 +/- 1 | 39 | 9.08 | 766 | 21.034 | 4 |
| 800 | 23 | 12 | 78 +/- 2 | 53 | 7.004 | 553 | 13.57 | 3 |
| 850 | 8 | 4 | 87 +/- 3 | 59 | 10.054 | 502 | 9.761 | 4 |
| 900 | 10 | 5 | 80 +/- 4 | 72 | 11.289 | 410 | 5.889 | 1 |
| 950 | 6 | 3 | 80 +/- 6 | 80 | 15.143 | 371 | 3.916 | 7 |
| 1000 | 7 | 4 | 67 +/- 5 | 80 | 24.078 | 368 | 4.431 | 13 |
| 1050 | 6 | 3 | 115 +/- 6 | 73 | 41.894 | 407 | 3.938 | 14 |
| 1100 | 10 | 5 | 107 +/- 4 | 63 | 78.44 | 467 | 6.56 | 28 |

TOTAL GAS AGE = 79 Ma

J = 2.34E-03

ERROR ESTIMATES AT ONE SIGMA LEVEL

37/39,40/36 AND 39/36 Ar RATIOS ARE CORRECTED FOR INTERFERING ISOTOPES

% IIC - INTERFERING ISOTOPES CORRECTION

# AX90-72 WHOLE ROCK SUMMARY (C2)

| °C | mV 39 | % 39 | AGE(Ma) | % ATMOS | 37/39 | 40/36 | 39/36 | % IIC |
|---|---|---|---|---|---|---|---|---|
| 500 | 22 | 2 | 89 +/- 2 | 56 | 1.693 | 531 | 10.855 | 1 |
| 600 | 62 | 7 | 104 +/- 1 | 32 | 1.723 | 909 | 24.123 | 1 |
| 700 | 136 | 15 | 89 +/- 1 | 40 | 1.86 | 738 | 20.562 | 1 |
| 750 | 100 | 11 | 94 +/- 1 | 28 | 1.613 | 1069 | 33.68 | 1 |
| 800 | 140 | 15 | 92 +/- 1 | 21 | 1.798 | 1390 | 48.806 | 1 |
| 850 | 110 | 12 | 91 +/- 1 | 31 | 1.788 | 968 | 30.248 | 1 |
| 900 | 78 | 9 | 95 +/- 1 | 26 | 1.562 | 1133 | 36.157 | 1 |
| 950 | 64 | 7 | 91 +/- 1 | 24 | 1.583 | 1249 | 43.339 | 1 |
| 1000 | 82 | 9 | 89 +/- 1 | 25 | 2.075 | 1205 | 42.305 | 1 |
| 1050 | 66 | 7 | 91 +/- 1 | 25 | 4.529 | 1178 | 39.84 | 2 |
| 1100 | 32 | 4 | 95 +/- 2 | 49 | 22.348 | 598 | 13.022 | 9 |
| 1200 | 18 | 2 | 122 +/- 3 | 57 | 41.599 | 541 | 8.185 | 13 |

TOTAL GAS AGE = 93 Ma

J = 2.34E-03

ERROR ESTIMATES AT ONE SIGMA LEVEL

37/39,40/36 AND 39/36 Ar RATIOS ARE CORRECTED FOR INTERFERING ISOTOPES

% IIC - INTERFERING ISOTOPES CORRECTION